Nano Today (2016) 11, 168—188

Available online at www.sciencedirect.com

ScienceDirect

journal homepage: www.elsevier.com/locate/nanotoday

REVIEW

Plasmonic nanoparticles in biomedicine

Wan Qi Lim, Zhiqiang Gao*

Department of Chemistry, National University of Singapore, Singapore 117543, Singapore

Received 24 November 2015; accepted 1 February 2016
Available online 24 March 2016

KEYWORDS
Plasmonics;
Nanoparticles;
Biosensors;
Photothermal therapy;
Drug delivery

Summary The use of plasmonic nanoparticles for biomedical applications has been extensively researched, yielding significant advancements in the construction of ultrasensitive bioassays and effective therapy. The unique surface plasmon resonance phenomena of both plasmonic films and nanoparticles with their exceptional absorption and scattering abilities have much potential in revolutionising diagnosis, treatment and evaluation of diseases, in particular cancer. In this review, an overview of recent advancements of plasmonic nanoparticles in the fields of bioassays and therapy is provided, with an emphasis on the mechanisms by which the plasmonic nanoparticles can be employed to enhance or provide signals for the detection of bioanalytes or to treat diseases.
© 2016 Elsevier Ltd. All rights reserved.

Introduction

Metallic nanostructures have been of particular interest due to their ability to interact with electromagnetic radiation, making them suitable for many biomedical applications, including diagnostics [1,2], therapeutics [3,4] and even the alteration of gene expression [5,6]. The ability of metallic nanostructures to interact with electromagnetic radiation stems from their confinement of electrons to produce quantum effects [7]. One of such effects is the surface plasmon resonance phenomenon, whereby incident light striking thin metal films or nanostructures causes the collective oscillation of electrons at a resonant frequency in these metal films or nanostructures [8]. This results in the intense absorption or scattering of light by the metallic nanostructures, which when coupled to fluorophores or Raman-active molecules, give rise to phenomena like metal-enhanced fluorescence [9] and surface-enhanced Raman scattering [10]. By increasing the intensities of existing signals of fluorescent or Raman labels, assays which employ these labels, for example immunoassays and nucleic acid assays, can have greatly enhanced sensitivities should plasmonic films or nanoparticles be introduced. In addition, plasmonic films or nanostructures can themselves act as sensors by transducing changes in bulk or local refractive index into shifts of their plasmonic bands of absorption in their UV-visible spectra [11]. Such an approach avoids the need for labelling of target analytes with fluorophores or Raman labels, of which blinking and bleaching are problems associated with the former [12,13]. Intense absorption of near-infrared radiation by the metallic nanostructures also causes photothermal heating of their surroundings and the generation of radicals that can be used for therapeutic applications [14,15]. Noble

* Corresponding author. Tel.: +65 6516 3887; fax: +65 6779 1691.
E-mail address: chmgaoz@nus.edu.sg (Z. Gao).

http://dx.doi.org/10.1016/j.nantod.2016.02.002
1748-0132/© 2016 Elsevier Ltd. All rights reserved.

metal plasmonic nanostructures like gold and silver nanoparticles are most commonly used due to their relative inertness and visible and near-infrared absorption bands [16], with gold nanoparticles popular for its biocompatibility while silver nanoparticles have larger molar extinction coefficients, giving more sensitive assays [17]. This review focuses on offering a broad perspective for the use of plasmonic platforms in biomedicine like bioassays and therapy. In the following sections, the plasmonic platforms are reviewed with typical mechanisms for the plasmonic approach to biomedical applications. We hope that this article will provide a comprehensive coverage of current standings of this field and offer new perspectives into the development of plasmonic materials for more effective bioassays and therapy in biomedicine.

Bioassays

Metal-enhanced fluorescence

Plasmonic enhancement of fluorescence occurs due to the coupling of fluorophores to the strongly confined electromagnetic fields of plasmonic nanoparticles or plasmonic metal films [18]. These strongly confined electromagnetic fields are generated as a result of interaction between light and localised surface plasmons of plasmonic nanoparticles or surface plasmon polaritons for films. The plasmonic materials then relay the radiation outward, increasing the radiative scattering efficiency of the fluorophores [19]. More recently, interactions between plasmonic nanoparticles and fluorophores were explained by the radiating plasmon model, whereby the enhanced emissions and decreased lifetimes of the fluorophores are due to the coupling of the fluorophores at their excited states with surface plasmons of the nanoparticles [18]. For the construction of metal-enhanced fluorescence assays, the distance-dependence of metal-enhanced fluorescence has been extensively employed. To further improve the sensitivity of metal-enhanced fluorescence, different strategies targeting the individual components of fluorescence assays have been developed. Also, studies have also been done to improve the practicality of such fluorescence assays.

Bioassays based on distance-dependence of metal-enhanced fluorescence

The fluorescence enhancement by plasmonic nanoparticles or plasmonic films has been shown to be dependent on the distance between the fluorophore and the plasmonic nanostructure [20]. Quenching occurs when the fluorophore is close to the plasmonic surface, while fluorescence is greatly enhanced when the distance between the fluorophore and the plasmonic surface increases beyond the quenching distance [21]. To study such distance-dependence, numerous approaches have been proposed to control the distance between the fluorophore and the plasmonic surface [21—28]. These include the use of DNA spacers [22,23], the layer-by-layer technique [27,28] and the deposition of and SiO_2 [28]. These approaches, however, are limited in the control of the thickness of the spacers. Chi et al. used the polymerisation of oligo(ethylene glycol)methacrylate to deposit thin polymer films on gold, a highly controllable process, to study the distance-dependence of metal-enhanced fluorescence of gold [29]. Fluorescence was found to be quenched when the fluorophore and the gold surface were 15 nm apart, while fluorescence enhancement was observed with an increase in the polymer thickness beyond the quenching range for films that are tens of nanometres thick, with a maximum enhancement with a 39-nm thick film.

Two different approaches exist for the use of the distance-dependent property of metal-enhanced fluorescence for bioassays, namely the quenching-to-coupling approach [22,30,31] and the signal enhancement approach [32,33]. The quenching-to-coupling approach refers to a 'molecular beacon-like' approach whereby a single molecule, usually DNA, conjugated to a fluorophore acts like a molecular beacon, with initial quenching of the fluorophore due to close proximity of the DNA—fluorophore conjugate to the plasmonic nanostructure. Subsequently, the molecule of interest binds, resulting in a change in the configuration of the DNA holding the fluorophore and the increase in distance between the fluorophore and the plasmonic nanostructure, resulting in coupling and hence de-quenching [22]. Some examples include that reported by Peng et al. who demonstrated the use of a DNA hairpin probe conjugated to a fluorophore and bound to silver nanoparticles immobilised on a glass slide [34]. The fluorophore was thus quenched in the absence of the target DNA due to its close proximity to the silver nanoparticles while fluorescence was restored with the hybridisation of the target DNA as the hairpin DNA changed its configuration, moving the fluorophore away from the surface of the silver nanoparticles. Li et al. reported the potential-dependence of the reorientation of DNA being investigated by metal-enhanced fluorescence [35]. Applying a positive potential caused the double-stranded DNA conjugated to the fluorophore lying on the electrode surface, thus resulting in fluorescence quenching, whereas, a negative potential resulted in the perpendicular arrangement of the DNA—fluorophore conjugate and the restoration of fluorescence. However, in addition to the large increase or decrease in fluorescence intensity, a slow relaxation process occurred whereby fluorescence intensities were restored to intermediate values (Fig. 1). Such findings may be able to facilitate advanced electrochemical detection of DNA in future. Moreover, Degliangeli reported the direct detection and quantification of microRNA with a very low limit of detection of 0.2 fmol without any target amplification [36]. This was performed using DNA probes conjugated to a fluorophore which were immobilised onto gold nanoparticles. In the absence of a target microRNA, the fluorophore remained close to the gold nanoparticles and its fluorescence was quenched. In the presence of the target microRNA, the DNA-microRNA hetero-duplex was formed and cleaved off the gold nanoparticles by the endonuclease duplex specific nuclease. Such cleavage resulted in the diffusion of the fluorophore away from the gold nanoparticles, allowing the fluorescence signal to be observed. Signal enhancement can also occur as microRNA remains intact after cleavage as shown by the attainment of the maximum fluorescence intensity whether microRNA was added in excess or in defect. Given that the fluorescence maximum was reached

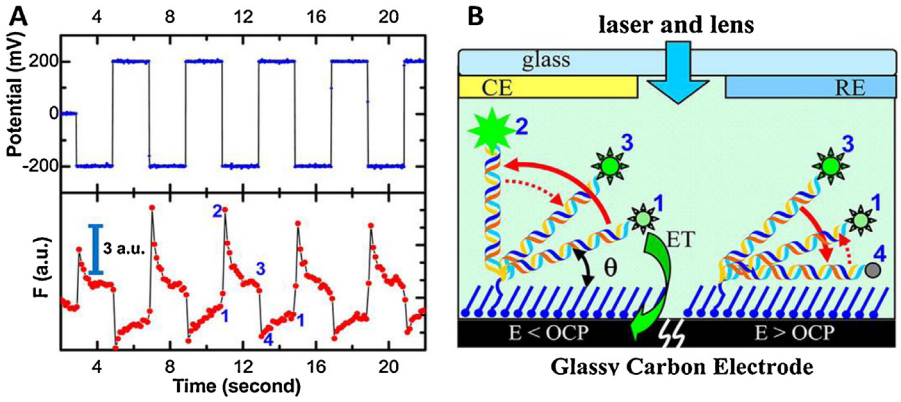

Figure 1 (A) Potential waveform applied to a glassy carbon electrode (top) and the resulting fluorescence intensity (bottom) and (B) the schematic of the optical and electrochemical cell with a model of the orientation of the double-stranded DNA.
Adapted from [35] with permission from American Chemical Society.

for all microRNA concentrations, the microRNA was quantified by measuring the fluorescence intensity after 2 h. It was thus possible to quantify microRNA down to 1×10^4 copies/ng_{RNA}.

The second approach is the signal enhancement approach, whereby fluorophore-conjugated biomolecules are immobilised onto the plasmonic surface through bioaffinitive interactions such as antibody-antigen interaction and nucleic acid base-pairing, resulting in the enhancement of fluorescence. The most common application of the signal enhancement approach is the use of spacers to enhance fluorescence for improving the sensitivity of bioassays [37,38]. More complicated arrangements have since been devised, one of which was utilised to investigate carbohydrate—lectin interactions [39]. Boronic acid tagged with a fluorophore interacts with gold nanoparticles encapsulated with carbohydrates in the absence of lectin, quenching the fluorescence. In the presence of carbohydrate-specific lectin, the boronic acid—fluorophore conjugates are released and the fluorescence recovers. The limit of detection of the plant lectin *Concanavalin ensiformis* was found to be 4.9 nM. Uptake of fluorescein—boronic acid attached to mannose-modified gold nanoparticles by the cancer cells were also demonstrated, while pure fluorescein—boronic acid was not taken up by cancer cells, implying that the possibility of the mannose-modified gold nanoparticles can be used as a non-covalent drug carrier. The use of fluorophore-conjugated biomolecules for the detection of proteins by immunoassays through metal-enhanced fluorescence was extensively explored. A variety of procedures were reported to achieve different purposes, some of which solely involved coupling between the fluorophore and plasmonic nanoparticles, for example where the procedures similar to sandwich immunoassays and hybridisation-based DNA assays were reported by Lee et al. using quantum dots and gold nanoparticles on carbon nanotubes [40] or by Cao et al. using silica nanoparticle-encapsulated fluorophores to maximise distance-dependent coupling by occupying the entire coupling zone while avoiding fluorescence intensity deviations due to different analytes or inhomogeneity

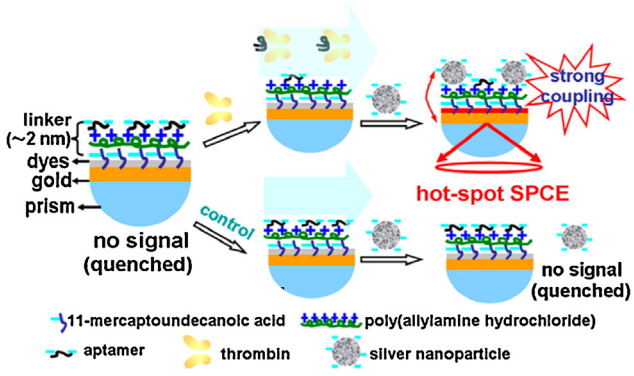

Figure 2 Schematic representation of the aptamer-based bioassay whereby strong plasmonic coupling occurs between the silver nanoparticles and the gold film, inducing high fluorescence emission.
Adapted from [43] with permission from American Chemical Society.

of the nanoparticle surface [41]. The coupling between a plasmonic film, plasmonic nanoparticles and a fluorophore were subsequently utilised, whereby the attachment of silver nanoparticles to a gold film with the fluorophore results in the turn-on of the fluorescence. This was both reported using a sandwich immunoassay configuration [42] and using target—aptamer interactions [43]. The latter used an ultra-thin linker layer composed of a layer of cationic polymers and a layer of aptamers specific for thrombin deposited successively on a gold film coated with the fluorophore. Such a layer maximises the sensitivity of the bioassay. This surface was initially negatively charged due to the presence of many negatively-charged aptamer strands. The negatively-charged silver nanoparticles were thus unable to bind and no fluorescence signal was detected as the fluorophore is quenched. In the presence of thrombin however, the aptamer binds to thrombin and consequently desorbed from the gold film, leaving the gold film positively charged due to the cationic polymers. The silver nanoparticles were hence able to bind, giving rise to enormous plasmonic coupling to

generate surface plasmon coupled emission (Fig. 2). Such a surface plasmon coupled emission is directional, with the emission of p-polarised light 46 degrees to the normal.

Improving sensitivity via other components of fluorescent bioassays

Other than the distance-dependence of metal-enhanced fluorescence for sensitivity improvement, strategies targeting the fluorophore, bioaffinitive agents, the antibody surface as well as the type of plasmonic film have been explored. Deng et al. proposed the use of lanthanide fluorophores like europium with long fluorescence lifetimes such that a high background rejection can be achieved [44]. By adding a europium chelate into a silver/silica core—shell nanocomposite, a maximum fluorescence enhancement of 9.5-fold was obtained. Despite a decrease in fluorescence lifetime accompanying the increase in fluorescence enhancement of the core/shell nanocomposite, the fluorescence lifetime of the europium chelate doped nanocomposite was still found to be much longer than that of cellular auto-fluorescence, thus allowing for the use of such lanthanide-doped plasmonic nanocomposites for cellular applications. In addition, at high intensities of excitation light, fluorescence enhancement factors significantly increased up to 146 folds for the europium chelate doped nanocomposite due to the fluorescence saturation in control samples while no fluorescence saturation was observed with the europium chelate doped nanocomposite. This is because the decay rate was found to be higher for the europium chelate doped nanocomposite than that of its non-doped counterpart.

Similarly, a homogeneously and densely packed capture antibody layer, which is often lacking in many immunoassays, can significantly improve the sensitivity of the assay as shown by Tawa et al. with a bispecific antibody for a ZnO film on one side and the analyte, epidermal growth factor (EGFR), on the other [45]. The need for a blocking agent was eliminated. Grating-coupled surface plasmon resonance was utilised for the sensitive detection of EGFR by using a grating coated with chromium, silver, chromium and then ZnO on the top layer. EGFR was then labelled with a fluorophore Cy5. Reverse coupling between the plasmon polaritons and Cy5 led to a fluorescence enhancement of up to 300 times as compared to the ZnO film, due to the high density of the bispecific antibody on the surface of the ZnO film, the exact regularity in the repeated structure and the optimal duty ratio. The limit of detection for EFGR was found to be 700 fM with a dynamic range between 10^{-13} and 10^{-8} M.

The use of different plasmonic films or nanoparticles was also investigated to improve the sensitivity of metal-enhanced fluorescence-based bioassays, for example with plasmonic nanostructures of different materials like aluminium nanoparticles [46] and bimetallic nanoparticles [47].

Practicality of metal-enhanced fluorescence assays

The practicality of metal-enhanced fluorescence to widen bioassay applications was improved, for example flow cytometry, whereby the analytes need not be immobilised onto the plasmonic film or nanoparticles as reported by Chowdhury et al. [48] and Deng et al. [49] or for the simpler fabrication of plasmonic film for the enhancement of fluorescence as shown by Szmacinski et al. [50].

Surface plasmon resonance and localised surface plasmon resonance assays

Surface plasmons refer to the coherent oscillations of conduction electrons on a metal surface when excited by electromagnetic radiation at the interface between a metal and a dielectric [51,52]. Two surface plasmon modes are usually employed: propagating surface plasmon resonance (PSPR) at flat smooth metal—dielectric interfaces [53] and localised surface plasmon resonance (LSPR) when surface plasmons are confined on either periodic [54], colloidal [55] or other nano-systems [56]. PSPR-based bioassays work by coupling a metallic thin film to a prism or a grating [51]. Surface plasmon polaritons excited by electromagnetic radiation then propagate along the metal surface with an electric field that decays exponentially from the metal—dielectric interface. Refractive index changes above the metal film alter the plasmon resonance condition, which can be measured as changes in intensity, wavelength or angle [57]. Like PSPR, LSPR detects refractive index changes on the plasmonic surface. However, the electromagnetic field in LSPR is confined to the nanostructures or nanoparticles. Therefore, despite having a lower sensitivity to refractive index changes than PSPR, the strongly confined field of LSPR leads to comparable signals generated. Also, LSPR is not coupled to prisms or polarisers and thus it is more popular due to its simplicity and high miniaturisation [58]. The sensitivity of the LSPR-based bioassays depends on the shape of the nanoparticles, which are typically anisotropic nanoparticles such as nanorods, nanoshells and nanoprisms.

PSPR-based bioassays

To improve the sensitivity of PSPR-based bioassays, the sensing of the unique properties of the PSPR film other than the PSPR shift and the coupling of other plasmonic nanostructures to modify the field have been investigated like the work done by Yu and colleagues [59]. They studied the sensitivity of both the extraordinary emission and the surface plasmon resonance of corrugated gold films fabricated by nanoimprint lithography to refractive index changes. Two surface plasmon resonance bands were observed for the corrugated gold films: one between the gold film and the polycarbonate film that the gold was deposited on and the second between the gold film and the superstrate applied on it. The intensity of the extraordinary transmission was found to be dependent on the refractive index of the superstrate applied on the corrugated gold film, with a greater intensity observed as the refractive indexes of the polycarbonate film and the superstrate got closer to each other. The change in intensity of the extraordinary was found to have a sensitivity of up to 8.96 a.u./RIU, while the sensitivity of the redshift in the surface transmission plasmon band for the plasmon mode between the gold film and the superstrate was found to have a sensitivity of up to 812 nm/RIU. The latter was used for the quantification of cysteine.

Also, Feng et al. reported a nanoscale plasmonic interferometer synthesised by a slit between two grooves, whereby the grooves scatter the light beam striking into multi-frequency surface plasmon polaritons, which interfere with

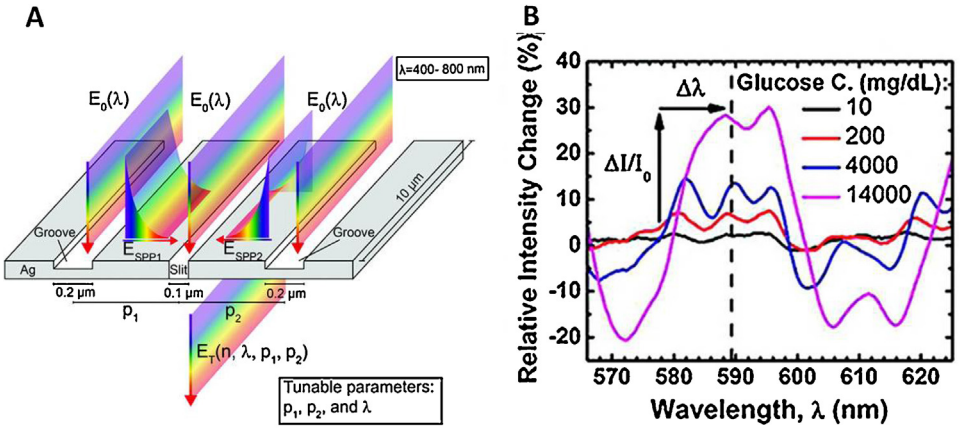

Figure 3 (A) Scheme showing the interference of surface plasmon polaritons on the transmittance of light through the slit and (B) relative intensity change with respect to wavelength in the presence of glucose.
Adapted from [60] with permission American Chemical Society.

the field at the slit and thus the transmittance of light through the slit [60]. This enabled generated surface plasmon polaritons to detect refractive indexes of solutions surrounding them. Depending on the wavelength of incident light, the light intensity transmitted through the interferometer can be increased or decreased (Fig. 3A). This paper thus showed the possibility of generating surface plasmon polaritons of all wavelengths with the groove at a fixed angle of incidence. Furthermore, this interferometer was used to sense glucose by patterning the interferometer into PDMS and then observing the intensity change at a fixed groove-slit length. The addition of glucose caused both an intensity change and a wavelength shift (Fig. 3B). The intensity change could be used to determine glucose concentration in a wider range (0.1—14,000 mg/dL) than that obtained with the wavelength shift (500—14,000 mg/dL). In addition, Zuccon et al. showed the inverse surface plasmon resonance with a palladium film which can be functionalised for bioassays with thiols or graphene [61].

The coupling of other plasmonic nanostructures has been shown by Law and colleagues [62]. To improve the sensitivity of the PSPR bioassay, they showed the effect of coupling a gold sensing film with gold nanorods to alter the evanescent electromagnetic field of the gold nanorods to achieve an enhanced SPR signal. Simulations indicated that without the gold nanorods, the field is weak and decreases exponentially with the distance from the film. The field is also confined within about 150 nm from the gold film. However, the evanescent field coupling between the sensing film and the gold nanorods placed within 150 nm of the gold film resulted in a very large enhancement in the electromagnetic field at the tips of the gold nanorods, with the largest increase in field when the gold nanorods and the gold film are 5 nm apart. The hypothesis was then tested out experimentally with a sandwich immunoassay for the detection of tumour necrosis factor alpha (TNF-α), whereby the sensing film was functionalised with TNF-α capture antibody while the gold nanorods were conjugated to TNF-α detection antibody. The use of gold nanorod detection antibody conjugates as amplifiers resulted in a 40-fold increase in sensitivity with the lowest detectable concentration of TNF-α being 0.03 pM.

LSPR-based bioassays

Types of LSPR-based bioassays include those that measure the extent of the LSPR shift as well as those that use colourimetric detection, detecting a change in colour in the presence of a bio-analyte.

Of those that measure the extent of LSPR shift, different methods have been employed to increase the LSPR shift for more sensitive detection of bioanalytes. The morphology of the nanostructures was found to greatly affect the extent of LSPR shift, and the nanostructure morphologies have been modified differently for periodic nanoarrays as well as nanoparticles in solution.

Periodic nanoarrays are commonly used for bioassays due to their high sensitivity in local refractive index changes as compared to PSPR. Also, they do not require excitation using a prism or a grating. The possibility of modifying individual nanostructures of the periodic nanoarray offers opportunities for the enhancement of sensitivity for LSPR-based bioassays. These include nanohole arrays [34—36,63—65] nanoring arrays [66], nanoparticles assembled in a periodic manner on glass slides [67,68], nanoprisms [40—42,69—71] and other unique nanoarrays [72].

Gold nanohole arrays were reported to give high sensitivity, as shown by Niu et al. who carried out a large scale fabrication of gold nanohole arrays by nanosphere lithography and then used them for the detection of streptavidin through specific biotin-streptavidin interaction [63]. Binding of streptavidin gave an 8-nm redshift, which was increased by four folds to 30 nm with the conjugation of CdSe/ZnS core—shell quantum dots to streptavidin for the amplification of the signal. The amplification as a result of the attachment of the quantum dots was attributed to two reasons: firstly the increase in the number of sites for streptavidin binding, whereby carboxyl sites on the quantum dots allowed more streptavidin-capturing biotin to be immobilised and secondly, the partial overlap of the SPR band of the gold nanoholes with the absorption and emission spectra of the quantum dots, allowing the energy from the excited state of the quantum dots to be transferred to the gold nanoholes and coupled with the SPR mode of the gold nanoholes via a nano-metal surface energy transfer

mechanism. Im et al., too, used a periodic nanohole array for the sensing of exosomes but measuring the transmission of light through the nanoholes instead of total internal reflection allowing for the miniaturisation of the array and the fabrication of more densely packed arrays [64]. For exosome sensing, the nanoholes were functionalised with antibodies against exosome proteins. Specific binding of the exosomes to the array changed the local refractive index, which was monitored by wavelength shifts in a light spectrum or intensity changes at a fixed wavelength. A limit of detection was established to be ~3000 exosomes while additional gold nanospheres and gold nanostars with conjugated antibodies targeted to the exosomal proteins further amplified the signal by 20% and 300%, respectively. This array-based exosome detection was also proven to be faster, more sensitive and required smaller volumes of sample than enzyme-linked immunosorbent assay. Furthermore, both grating and nanohole arrays were studied by Oh et al. who reported the co-localisation of the localised evanescent field of a metal film and the interaction between complementary DNA strands in a plasmonic nanogap array for the detection of DNA [65]. This was done using oblique evaporation of a dielectric film on top of the grating or nanohole arrays with respective circular and triangular patterns, resulting in nanogaps at the bottom edge of the nanoholes. DNA was then co-localised in the nanogaps where the electromagnetic hotspots were. Large SPR angle shifts were observed with a large angle of oblique evaporation due to the large nanogaps synthesised. The relative angle shift, which is indicative of the overlap between the field and the localisation of the DNA, was found to be the highest at an oblique angle of 60°, 200 times that of the non-co-localised DNA in the same gaps. The detection sensitivity in terms of binding capacity was found to be 1.6 fg/mm^2.

Nanoprisms immobilised on glass substrates in a periodic manner were commonly used in bioassays [73]. For instance, Hall et al. reported the first conformational change of an unlabelled protein—calmodulin detected by LSPR [70]. This was performed using functionalised surface-confined antigen nanoprisms on a glass surface. A redshift of 0.96 ± 0.06 nm was then observed when calmodulin switched from its rigid dumbbell-like structure when bound to calcium to its more flexible structure when not bound to calcium. A reverse blueshift was observed for the closing of calmodulin. This was then used to detect calcium with a limit of detection of 23 μM. Joshi et al., on the other hand, fabricated a bioassay based on gold nanoprisms functionalised with single-stranded DNA probes for the detection of microRNA, with the nanoprisms immobilised on a glass slide [71]. A large redshift of 20.5 ± 3.2 nm was induced upon the binding of 100 nM of microRNA 21 due to the strong electromagnetic field of the gold nanoprisms and the significant change in refractive index with the formation of the DNA-microRNA duplex. The limit of detection was found to be between 23 and 35 fM for microRNA 21 depending on the media that the microRNA was dissolved in.

A unique gold mushroom array was fabricated by Shen et al. which gave a figure of merit of 108, comparable to the theoretical predicted upper limit for PSPR even though PSPR tends to have a higher figure of merit than that of LSPR [72]. The gold mushroom structures, which consisted of a gold cap on a photoresist pillar grounded in a hole in the gold film (Fig. 4), showed the coupling of LSPR with Wood's anomaly. This resulted in a low full width half maximum (10 nm) and a high refractive index sensitivity (1010 RIU^{-1}) due to the raised gold caps. The gold mushroom array was then used as a plasmonic bioassay, giving very low limits of detection for cytochrome c and α-fetoprotein of 200 pM and 15 ng mL^{-1}, respectively.

For nanostructures that are not constructed in a periodic manner, but rather dissolved in solution, the potential for creating different nanoparticle morphologies is even larger. The morphology of the nanoparticles, together with their composition, size and local dielectric environment affects their absorption and scattering spectra, especially at the wavelength they absorb maximally. Thus, different sensitivities to local refractive index are expected for different nanoparticle morphologies. Two types of detection modes are typically performed: direct analyte detection, whereby a shift is detected when the analyte binds, and colourimetric detection, whereby the solution undergoes a colour change when the analyte is present.

For the direct detection of an analyte through the shift in the plasmonic band when the analyte binds, two main threads of research were taken. The first involves the search for unique morphologies of nanostructures which can give larger LSPR shifts than common nanospheres. Gold nanocages are hollow plasmonic nanostructures which have highly tuneable plasmonic nanostructures into the near infrared region and being hollow, give higher refractive index sensitivities than solid ones. Tian et al. reported the higher refractive index sensitivity of gold nanocages of 327.3 nm RIU^{-1} as compared to nanorods (207 nm RIU^{-1}) or nanoparticles [74]. The narrow plasmonic band of the gold nanocages gave a high figure of merit of 2.7. The gold nanocages were also more sensitive to local refractive index changes than the gold nanorods, with a higher electromagnetic decay length of 10.0 nm. The gold nanocages were thus employed in the detection of neutrophil gelatinase-associated lipocalin, capable of detecting lipocalin at 25 ng mL^{-1}. The use of multi-block gold-silver nanorods instead of pure nanorods for dopamine detection was investigated by Choi et al. [75]. The multi-block nanorods gave a larger shift in response to dopamine binding than that of pure gold nanorods. The binding of dopamine onto the pure gold nanorods that were coated with dopamine antibodies gave shifts of 10 nm and 16 nm in the quadrupole longitudinal mode for the 200 nm and 596 nm long nanorods, respectively. The triblock gold-silver-gold nanorods, however, gave larger shifts of 21 nm and 36 nm for total nanorod lengths of 546 nm and 589 nm, respectively, with larger shifts observed with an increase in the proportional length of silver. This is because silver has a higher optical sensitivity to a change in refractive index of the surroundings than gold. The number of junctions was found to have a greater effect on the redshift of the longitudinal surface plasmon band than the proportional length of the silver because surface plasmon coupling between the silver and gold portions would be affected by molecular interactions. With the increase in the number of junctions, coherent oscillation of electrons would thus be more disturbed by molecular adsorption.

The second thread is the advent of the single nanoparticle plasmonic bioassay as described by Seo et al. [76] and Hu et al. [77]. Seo et al. reported the monitoring of the catalytic

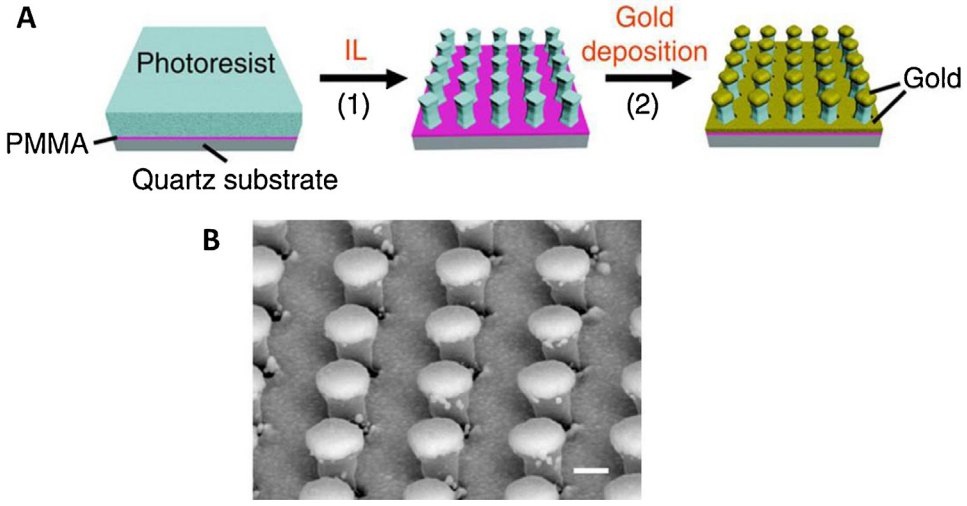

Figure 4 (A) Schematic illustration of the formation of the gold mushroom array (IL stands for interference lithography, gold caps are raised by dielectric pillars with low refractive index) and (B) scanning electron microscope image of the gold mushroom array. Adapted from [72] with permission from Nature Publishing Group.

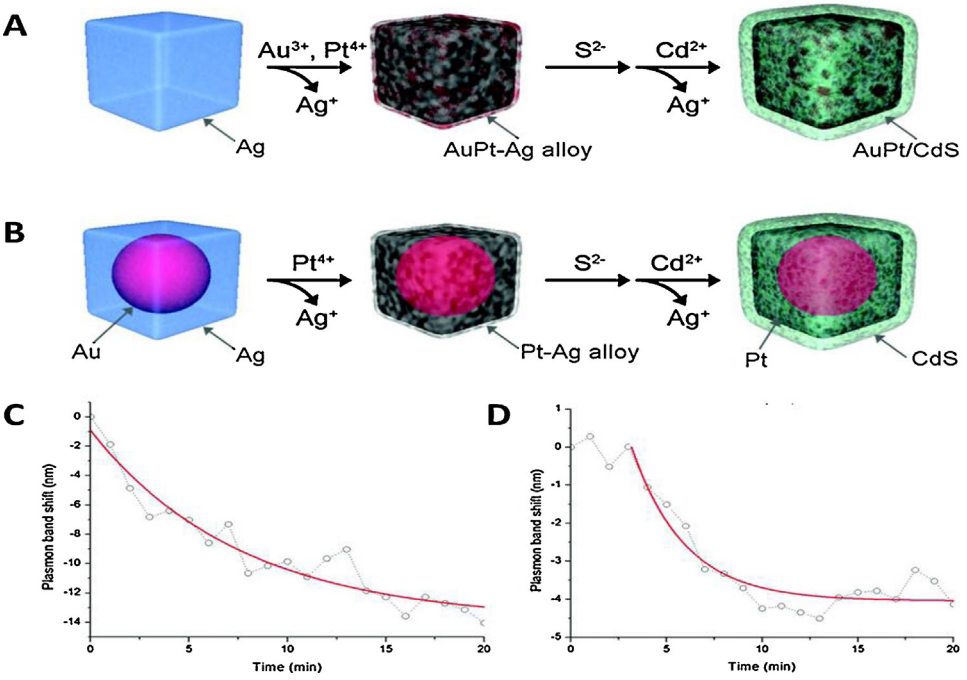

Figure 5 (A) Schematic illustration of the formation of AuPt/CdS cubes, (B) schematic of the formation of Au@Pt/CdS nanoparticle, (C) plasmon band shift of the AuPt/CdS cube upon hydrogen generation and (D) plasmon band shift of the Au@Pt/CdS nanoparticle upon hydrogen generation.
Adapted from [76] with permission from American Chemical Society.

hydrogen generation process [76]. To probe the reaction, two methods were used: the first was to locate gold domains near a platinum catalyst site by using gold-platinum/CdS hollow cube (AuPt/CdS) (Fig. 5A) while the second was to trap a gold nanoparticle in a Pt/CdS cube (Au@Pt/CdS) (Fig. 5B). The former could result in interference of the platinum catalyst while the latter could not. The photocatalytic decomposition of lactic acid was monitored using dark-field microscopy of the single nanoparticles, which gave a 14-nm blueshift for the AuPt/CdS nanoparticles (Fig. 5C) and a 4.6-nm shift for the Au@Pt/CdS nanoparticles (Fig. 5D) due to the generation of hydrogen gas. As expected, the smaller shift of the Au@Pt/CdS nanoparticles is a result of the larger distance between the gold nanoparticles and the Pt/CdS nanocubes. Redshifts, however, were observed for some cubes due to the trapping of hydrogen gas in the cube. This was temporal as the accumulation of hydrogen gas led to its escape and the system returned to equilibrium. Single nanoparticle bioassays were also reported by Hu et al. for the detection of DNA and microRNA [77]. Hairpin DNAs were

first conjugated on the surface of single gold nanoparticles, after which the binding of target DNA or microRNA led to the breaking of the hairpin structure, resulting in a redshift in the LSPR spectrum. The limits of detection for both DNA and microRNA were found to be 3 nM. The bioassay was also found to be highly specific to target microRNA.

Colourimetric detections of bioanalytes are also possible, which can be done without the need for expensive and bulky instruments. Selective removal [78], synthesis [79], aggregation [50—57,80—88], etching [58—61,89—92] and coating of plasmonic nanostructures [62—64,93—95] have been proven to be viable strategies of achieving a colour change through changing the morphology of the plasmonic nanoparticles.

Many bioassays use the redshift of gold nanoparticles during aggregation for the detection of biomolecules. Such a redshift has been found to be due to the coupling of the surface plasmonic resonance bands of the gold nanoparticles as they aggregate. However, to prevent nonspecific binding of biomolecules, the gold nanoparticles are often coated with a silica shell. The effect of the thickness of the silica shells on the redshift upon aggregation was thus studied by Vanderkooy et al. who synthesised silica shells of different thickness using tetraethylorthosilicate or diglyceroxysilane [80]. Thin silica shells on the gold nanoparticles were found to give a large redshift of the nanoparticles during aggregation, while thick silica shells led to a small redshift of the nanoparticles. Aggregation of plasmonic nanoparticles for colourimetric detection is often catalysed by enzymes. For example, Nie et al. reported the ultrasensitive detection of Treponema pallidum using a plasmonic enzyme-linked immunosorbent assay [81]. This was performed using biotinylated acetylcholinesterase which was immobilised on the well in the presence of the Treponema pallidum antigen. Acetylcholinesterase catalysed the conversion of acetylthiocholine to thiocholine. The thiol group on thiocholine then facilitated its binding to the surface of the gold nanoparticles. This caused some positive charges to be generated on the surface of the gold nanoparticles, resulting in attraction and the coupling of the localised surface plasmon resonance bands between the gold nanoparticles. A redshift from 520 nm to 700 nm thus occurred, causing the solution to change from red to blue. The limit of detection of the bioassay was found to be 0.98 pg/mL. Moreover, de la Rica et al. reported a red to blue colour change using a similar sandwich immunoassay for the detection of prostate-specific antigen and human immunodeficiency virus capsid antigen p24, but with a different mechanism [82]. In the absence of the antigen, it was found that hydrogen peroxide effectively prevents the aggregation of the gold nanoparticles. Upon antigen binding to the capture antibody in the well, catalase-conjugated streptavidin, was then immobilised on the well, catalysing the disproportionation of hydrogen peroxide, thus causing the aggregation of the gold nanoparticles. The limits of detection of both prostate-specific antigen and p24 were found to be 10^{-18} g mL^{-1}. Not only can nanoparticle aggregation be controlled by enzymes, but also enzyme mimics like horseradish peroxidase-mimicking DNAzyme can be used, as shown by Niazov-Elkan et al. whereby L-cysteine, the analyte, is able to cause aggregation of the gold nanoparticles in the absence of the DNAzyme, while in the presence of the DNAzyme, aerobic oxidation of L-cysteine to cysteine inhibits aggregation [83]. The detection of target DNA was performed by constructing a hairpin DNA consisting of the enclosed and inactive configuration of the G-quadruplex, part of the DNAzyme, and the complementary DNA sequence to the target. The binding of the target DNA opened the hairpin DNA, allowing the self-assembly of the G-quadruplex and binding of hemin to form the DNAzyme and thus inhibiting aggregation. Aggregation can also be enzyme-free as demonstrated by Wang et al. [84] and Guo et al. [85]. Wang et al. used an aptamer for the detection of ATP, whereby the aptamer specific for ATP was bound to its complementary strand in the absence of ATP, leading to the aggregation of the gold nanoparticles [84]. The presence of ATP frees the aptamer from its complementary strand, causing the single-stranded complementary DNA to bind to the gold nanoparticles and stabilise them, hence preventing their aggregation. For aggregation-based bioassays, however, the sensitivity, dynamic range and stability are usually limited by the formation of large nanoparticle aggregates. Guo et al. thus demonstrated the specific generation of nanoparticle dimers upon target DNA binding [85]. A Y-shaped duplex was generated when the detection probe and capture probe, each bound to an asymmetrically polyethylene glycol-modified gold nanoparticle, binds to the target DNA (Fig. 6A). The asymmetrical PEG-modified gold nanoparticles result in only dimer formation, ensuring the stability and a wide dynamic range, whereby the dynamic range of the bioassay was from 1.0 pM to 10 nM as compared to 10 nM to 300 nM for the conventional bioassays. Such a duplex also minimises the interparticle distance of the two gold nanoparticles, maximising the LSPR shift and the plasmonic coupling of the two gold nanoparticles, which was demonstrated by the appearance of a second peak at about 600 nm (Fig. 6B). The absorbance of the sharp peak at 600 nm increased with increasing concentration of the target DNA, also leading to a colour change from red to blue. The limit of detection obtained for such a bioassay was 10,000 times lower than those of conventional bioassays utilising gold nanoparticles symmetrically modified with probe molecules. Similarly, Shen and co-workers reported a colourimetric bioassay for ultrasensitive detection of DNA [87]. Leveraging on the amplification power of ligation chain reaction (LCR) and its ability to join two DNA strands together, gold nanoparticles coated with oligonucleotides complementary to a target DNA were successfully ligated together during the LCR, thus leading to a significant redshift. A detection limit of 20 aM with a selectivity factor of 1000 was achieved after 30 cycles of the LCR.

Colourimetric detection could also be performed by etching of existing nanoparticles to generate a colour change. In two recent studies [89,92], Yang et al. demonstrated the etching of triangular silver nanoprisms [92]. In the first study, etching of silver nanoprisms was performed by hydrogen sulphide which was also the analyte, whereby the increase in hydrogen sulphide concentration resulted in a decrease in absorbance and a redshift of the SPR peak of the silver nanoprisms as they were etched. The second study showed enzyme-assisted etching for the detection of DNA at concentrations as low as 6.0 fM [89]. As shown in Fig. 7, DNA hybridisation chain reaction was performed with two hairpin DNA strands — H1 and H2. H1 was biotinylated and H2 was not biotinylated. In the presence of a target DNA,

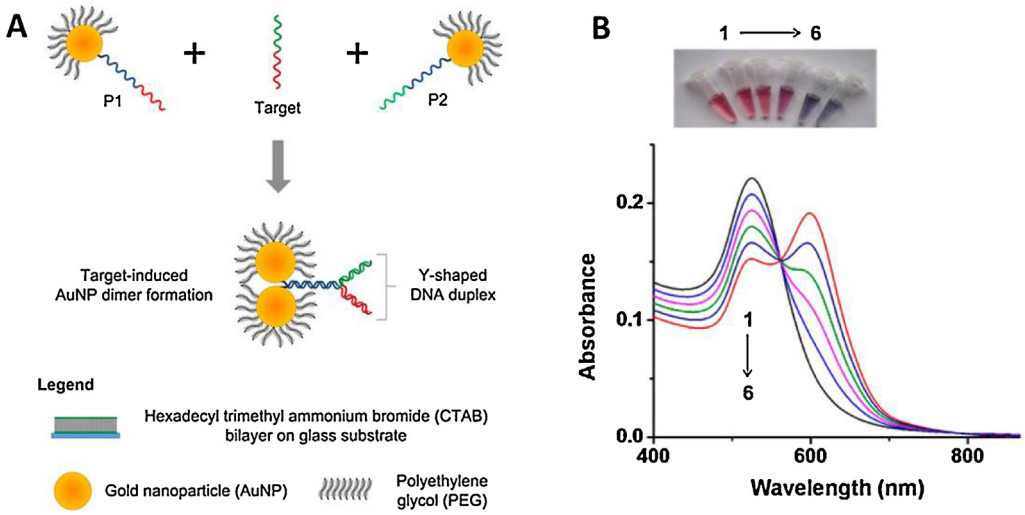

Figure 6 (A) Schematic representation of the formation of nanoparticle dimers upon target DNA binding using the asymmetrical polyethylene glycol-modified gold nanoparticles and (B) photograph and optical absorption spectra of the asymmetrically-modified gold nanoparticles at increasing concentrations of target DNA.
Adapted from [85] with permission from American Chemical Society.

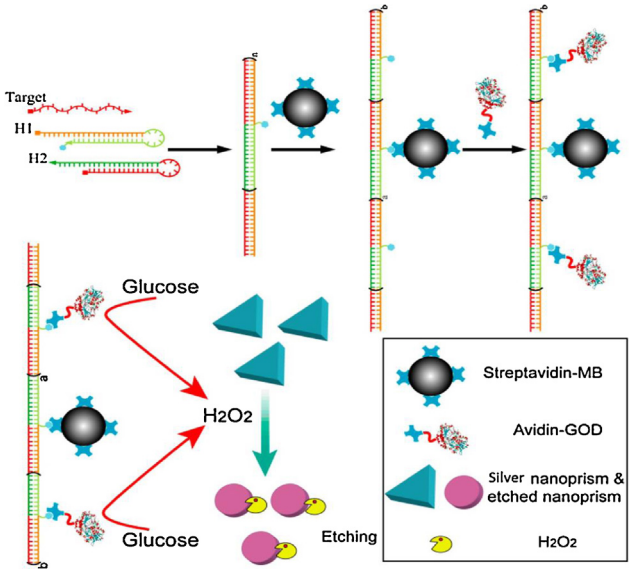

Figure 7 Schematic illustration of the construction of an etching assay for the detection of target DNA.
Adapted from [89] with permission from American Chemical Society.

H1 was opened when the target DNA displaced the double-stranded part of the hairpin and H2, containing a blocked DNA sequence, was then opened triggered by the release of the single strand in H1, resulting in nicked, linear and long double-stranded DNA strands with numerous repeated units which were biotinylated. Streptavidin-coated magnetic beads were then used to isolate these DNA strands and streptavidin-tagged glucose oxidase interacted with the rest of the biotin sites. In the presence of glucose, molecular oxygen was converted to hydrogen peroxide. Hydrogen peroxide was then used to etch the triangular silver nanoprisms into smaller spherical silver nanoparticles, which exhibited a significant blueshift in SPR peak (Fig. 7). It was observed that the magnitude of the blueshift is directly associated with the concentration of the target DNS.

Malile et al. also demonstrated the analyte-induced etching of silver nanoparticles for the colourimetric detection of bioanalytes but employing a gated mechanism for the etching of the silver nanoparticles [90]. This was conducted with a polyelectrolyte film containing DNA aptamer coated on top of gold-coated silver nanoprisms on a glass substrate. Binding of the analyte, sulforhodamine B, a fluorescent dye, to its aptamer on the polyelectrolyte film led to a change in the conformation of the aptamer and a change in the electrostatic balance of the polyelectrolyte film, causing the permeability of the polyelectrolyte film to increase and allowing the etching agent to enter. The etching of the nanoprisms caused a significant redshift of 84 nm in the presence of only 10 μM sulforhodamine B.

Additionally, coating of plasmonic nanostructures has also been shown to be a viable approach for colourimetric detection. Unlike aggregation-based assays, which are often affected by the ionic strength and impurities in complicated matrices, the enzymatic coating of plasmonic nanoparticles is less affected by the matrices of real-world samples. This was separately confirmed by Zhou et al. [93], Yang et al. [94] and Rodriguez-Lorenzo et al. [95]. Both Zhou [93] and Yang [94] reported the detection of antigen with p-aminophenyl phosphate and alkaline phosphatase for the silver coating of gold nanostructures. The former using gold nanoparticles while the latter using gold nanorods. Zhou used the increase in absorbance at 370 nm to quantify avian influenza viruses [93], while Yang reported the sensing of prostate-specific antigen using the blueshift of the longitudinal plasmon band of the gold nanorods [94]. Yang achieved a 10^4-fold improvement in sensitivity for prostate-specific antigen as compared to conventional enzyme-linked immunosorbent assay [94]. On the other hand, Rodriguez-Lorenzo et al. employed sil-

ver coating of gold nanostars to construct a colourimetric bioassay for prostate-specific antigen [95]. In the presence of low concentrations of prostate-specific antigen, low concentrations of glucose oxidase were immobilised, resulting in low concentrations of hydrogen peroxide generated. With low concentrations of hydrogen peroxide, silver ions were reduced to metallic silver and coated the gold nanostars, resulting in a large shift in the LSPR band of the gold nanostars. With high concentrations of prostate-specific antigen, however, the high concentrations of hydrogen peroxide generated triggered the excessive reduction of silver ions into metallic silver to form free-standing silver nanoparticles, thereby resulting in a small shift in the LSPR band of the gold nanostars. As a result, a limit of detection of 10^{-18} g mL^{-1} was achieved.

While much effort has been devoted to increasing the sensitivity of LSPR bioassays, some have also investigated the practicality of such LSPR bioassays, such as its implementation in microfluidic devices for high throughput applications as shown by Sadabadi and colleagues [96]. They investigated the in situ synthesis and immobilisation of gold nanoparticles in polydimethylsiloxane (PDMS) channels of a lab-on-a-chip device such that the LSPR properties of the gold nanoparticles could be used in biosensing in microfluidic devices. The reaction time for such a reaction, however, was long, with the saturation phase reached only after 5 days due to the slow migration time of the reducing agent for the reduction of gold (III) ions, which was also the crosslinking agent in the PDMS network. The gold nanoparticles synthesised in the microfluidic environment were found to have more uniform size than those synthesised in a macroenvironment. This gave sharper gold LSPR bands and more even coating of the antibodies onto the gold nanoparticles, which could improve the sensitivity of the bioassay. A detection limit of 3.7 ng/mL was found when using the bioassay to detect bovine growth hormone.

The use of natural antibodies conjugated to plasmonic nanoparticles for immunoassays can be a problem due to their extremely high cost and poor stability. Balamurugan et al. [97] suggested the use of aptamers to overcome this problem while Abbas et al. [98] proposed the imprinting of artificial antibodies using organosiloxane monomers trimethoxypropylsilane and (3-aminopropyl) trimethoxysilane in the presence of a target molecule. This was performed by modifying gold nanorod surface using p-aminothiophenol and glutaraldehyde to attach the target molecule. The organosiloxane monomers were then copolymerised onto the gold nanorod surface, followed by the removal of the target molecule. The sensitivity was further enhanced by the imprinting and hence the binding of the analyte at the plasmonic hotspots of the nanorods, which was favoured due to less coverage of the surfactant. The linear range of the bioassay was found to be between 1 and 6 μM of neutrophil gelatinase-associated lipocalin with a detection limit of 13 nM.

Plasmonic nanoparticles can also offer the capabilities of manipulating and sensing biomolecules like proteins and nucleic acids, opening up a completely new avenue for the development of biosensing platforms. Being comparable in size to the proteins and nucleic acids, changes in plasmonic properties of single nanoparticles may be monitored at single molecule level. The first attempt biosensing using single nanoparticles was reported in 2003 [99]. It was shown that binding of streptavidin onto biotinylated single gold nanoparticles in induced a detectable spectral shift of plasmon resonance. Later, another report demonstrated that the plasmon resonance Rayleigh scattering (PRRS) of individual nanoparticles are highly sensitive to changes in refractive index changes, thus resulting in measurable shifts in PRRS [100]. It was further demonstrated that both antibody-antigen interaction can be monitored in real time at single nanoparticle level. Later, several groups reported the detection of pathogen using gold nanoparticles [101], microRNA with silver nanocubes [102], and protein with gold nanorods [103]. For example, Ament et al. showed that single gold nanorods can be utilised to detect proteins label-freely with extremely high temporal resolution [103]. The high sensitivity and temporal resolution paves the way to study the dynamic evolution of biomolecule interactions on single gold nanorod surface at single molecule level.

Surface enhanced Raman scattering (SERS)

Raman scattering refers to the scattering of photons that are higher or lower in frequency as compared to the incident photon that strikes an analyte due to the vibrations and rotations of an analyte. A Raman spectrum is unique to the analyte and can be used for its identification, imaging and quantification. However, Raman signals are very weak due to the extremely small scattering cross-sections of Raman active molecules. SERS thus enhances the sensitivity of Raman bioassays for qualitative and quantitative detection of bioanalytes. Two mechanisms for the surface enhancement of Raman scattering by plasmonic nanostructures have been proposed, with the electromagnetic enhancement being more widely accepted as the one with the greater effect. Electromagnetic enhancement occurs due to LSPR of the nanoparticles concentrating the incident light, creating an intense local electromagnetic field. SERS signals are further increased when ''hotspots'' are formed, due to LSPR coupling of multiple nanoparticles. SERS can be performed with or without Raman labels, with the latter enhancing the intrinsic Raman signal of an analyte.

SERS with Raman labels

For effective enhancement of Raman signals, the control of the size of the nanogaps in which Raman labels reside is extremely crucial. Different methods were developed for this purpose, for example Chen et al. using high pressure sputtering to form a silver nanoparticle film with highly dense sub-10 nm gaps to which Raman-active molecules can bind for the enhancement of their Raman signals [104]. The sub-10 nm gaps were also found to be essential for the SERS enhancement due to the roughness of the surface providing a component of the SPR such that it is perpendicular to the surface for scattering, giving an enhancement factor of 1000 times that of a smooth Ag surface. Taylor et al., on the other hand, employed the gaps between dispersed gold nanoparticles [105]. To ensure the reproducibility of the gaps between the gold nanoparticles and placing the analyte molecules precisely in these gaps of high enhancement of Raman signals, Taylor used cucurbit[n]urils, a Raman-active host molecule with sub-nanometre dimension,

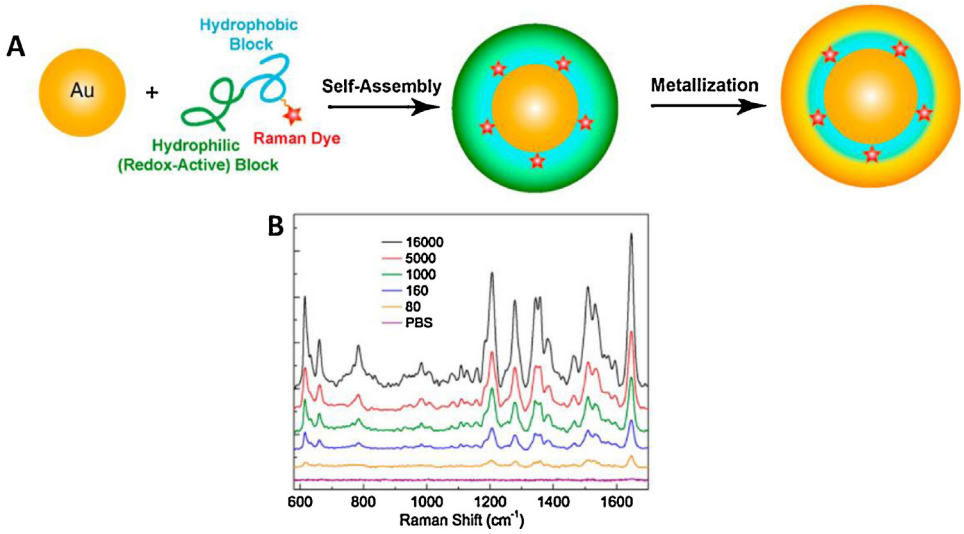

Figure 8 (A) Schematic illustration of the core—shell gold nanoparticle with the nanogap and (B) enhancement in Raman signals for the detection of MCF-7 breast cancer cells.
Adapted from [106] with permission from American Chemical Society.

aggregated with gold nanoparticles to give a repeatable and fixed 0.9 nm separation. Huge Raman enhancement factors of up to 10^{11} were obtained. Most uniquely, Song et al. reported the synthesis of core—shell gold nanoparticles with a nanoparticle-templated self-assembly of amphiphilic block copolymers, whereby the hydrophobic portion was tagged with a Raman label, while the hydrophilic portion consisting of redox active phenol groups, which subsequently reduces the gold precursor to form a shell (Fig. 8A) [106]. The nanogap in the sub-2 nm region can be customised while the confinement of the Raman reporter between the core and the shell instead of conjugating it to the outer surface of the nanoparticle prevents the loss of the Raman label's signal. The coupling between the core and the shell enabled high sensitivity for SERS imaging and detection with concentrations as low as 30 cells/mL of MCF-7 breast cancer cells detectable (Fig. 8B).

While Chen et al. [104], Taylor et al. [105] and Song et al. [106] reported short-range plasmonic coupling, long-range plasmonic coupling was studied by Qian and co-workers with gaps of up to 60 nm between gold nanoparticles for target DNA hybridisation [107]. By functionalising gold nanoparticles with malachite green, the reporter molecule, and then capture probes, SERS contrast ratios of 40—50 can be achieved. This suggests that SERS can be used in future to detect large molecules given than plasmonic coupling is not limited to short-range.

Manipulating the morphologies of plasmonic nanoparticles was also found to be a common strategy for enhancing SERS intensities, as investigated by Li et al. for both silver [108] and gold nanoparticles [109]. In the latter approach, gold nanospheres and gold nanostars were each covered with a layer of malachite green isothiocyanate and a layer of silicon dioxide. The modified gold nanospheres were respectively coupled with a planar gold film and a gold triangle nanoarray while the modified gold nanostars were coupled with a gold triangle nanoarray. Immunoglobulin G was then detected using a sandwich immunoassay involving the coupling of the gold nanoparticles and gold nanostructures, with the modified nanoparticles conjugated to the detection antibody while the nanostructure array was conjugated to the capture antibody. The modified gold nanostars on the gold triangle array showed the strongest SERS intensity, largely due to the increased probability of LSPR coupling. Such a bioassay gave a wide linear range from 0.1 pg/mL to 10 ng/mL and a low detection limit of 7 fg/mL for Immunoglobulin G. Furthermore, unique morphologies of silver nanoparticles were created by anisotropic etching of octahedral silver nanoparticles as reported by Mulvihill et al. [110]. Etching occurs largely in the (100) faces to form etched octahedral structures at low etchant concentrations and octapod structures at higher etchant concentrations (Fig. 9A). The etched octahedral structures gave the best enhancement at 633 nm excitation for single particle SERS spectroscopy, resulting in 5- to 50-fold increases in the SERS intensity of benzenethiol for the etched octahedral structures as compared to the parent octahedral structures (Fig. 9B). This was attributed to the unique interparticle gaps created upon etching, which allowed the etched nanoparticles, comprising of the etched octahedral and octapod structures, to perform as single nanoparticle SERS substrates.

On the other hand, stimuli-responsive SERS was found to be extremely important in bioassays applications. Stimuli includes both the responsivity of the bioassay to pH, as shown by Qian et al. [111], as well as to the analyte, whereby Raman enhancement was turned off and on as shown by Fabris et al. [112]. Qian fabricated a SERS bioassay whereby the Raman signals were stimuli-responsive, specifically pH-responsive [111]. Thiolated block copolymers made up of a pH-responsive segment of polymethacrylic acid (PMAA), an amphiphilic segment of polyethylene glycol and a lipoic acid for binding to gold nanoparticles were conjugated onto the gold nanoparticles with Raman reporters attached. At pH above 3, the copolymers were expanded due to their negatively charged carboxylic groups, causing PMAA to be

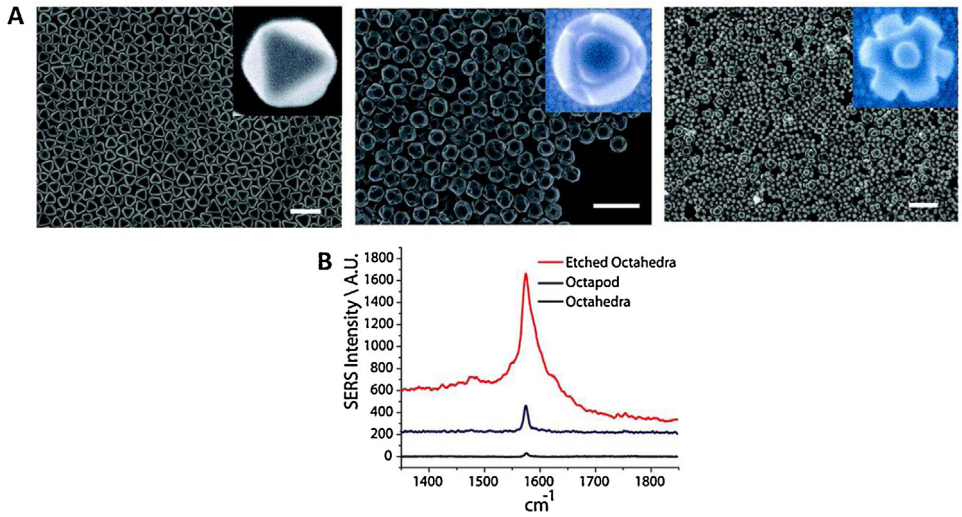

Figure 9 (A) Scanning electron microscopy images of octahedral silver nanoparticles (left), etched octahedral nanoparticles (middle) and octapod structures (right) and (B) the enhancement of SERS intensities in etched octahedral and octapod structures. Adapted from [110] with permission from American Chemical Society.

hydrophilic. However, at pH below 3, the PMAA groups become neutral, slightly hydrophobic and condensed. The amphiphilic polyethylene glycol groups were able to interact with the PMAA groups, further condensing the copolymer. The nanoparticles were thus closely aggregated, resulting in greatly enhanced SERS intensities by 30 to 35 times.

A turn-on/turn-off bioassay was fabricated by Fabris et al. using a PNA-based SERS method for the detection of complementary DNA [112]. Such a bioassay did not require the prefabrication of metallic nanostructures. In the presence of target DNA complementary to the PNA immobilised on a glass slide, target DNA hybridises, creating a net negative charge layer on the slide. Positively charged silver nanoparticles coated with dimethylaminopyridine then bind preferentially to the negatively charged slide, followed by the soaking of the slide in a Raman reporter solution. Raman enhancement was thus observed only in the presence of the target DNA, as the PNA slide without the target DNA is neutral and does not bind the silver nanoparticles. Excellent differentiation between the slide containing the target DNA and the slide without the target DNA was obtained.

Label-free SERS

Opto-fluidic chips have been used for the label-free detection of biomolecules. The intense SERS properties of plasmonic nanoparticles make them attractive for the modification of such opto-fluidic chips. However, the addition of plasmonic nanoparticles into the flow with the biomolecules lowers the reproducibility of the method due to the non-uniform spacing or the aggregation of the nanoparticles. Oh et al. thus reported the simple fabrication of silver coated micro-channel by evaporating silver onto the entire microchip surface, before removing those outside the microfluidic channels with adhesive tape [113]. The uncoated PDMS surface then facilitates the binding of the channel onto the glass plate by oxygen plasma, with the oxygen plasma also converting the silver film to silver nano-probes, increasing the roughness and thus increasing the intensity of SERS. Such a bioassay allowed the quantitation of dopamine by SERS. Kumar et al. reported the opto-fluidic sensing of 4-mercaptopyridine using periodic suspended Ag nanohole arrays (Fig. 10A), achieving Raman enhancement factors of up to 10^7 for the sensing of 4-mercaptopyridine and benzenethiol [114]. To tune the surface plasmon resonance for maximum enhancement of Raman signals, sucrose solution of an appropriate concentration was applied such that the SPR peak was shifted to 785 nm, which is equal to the frequency of the laser applied. The application of hydrophilic silica on one side of the chip allowed the solution to flow through the nanoholes (Fig. 10B), which could be applied for even more sensitive detection of 4-mercaptopyridine as 4-mercaptopyridine contains a thiol group, allowing it to be covalently immobilised or physically adsorbed on the plasmonic hotspots. This gave a very low detection limit of 272 amol.

In the targeting and sensing of biomolecules in solution, one important challenge would be to enable two distinct and powerful capabilities to operate with the same plasmonic particles, whereby the combination of LSPR with complementary molecular identification through SERS and other identification techniques would increase the reliability of the bioassays. Potara et al. reported the simultaneous use of both LSPR and SERS using chitosan-coated triangular silver nanoparticles [115]. Such nanoparticles were used to detect both adenine and para-aminothiophenol (p-ATP) via LSPR and SERS. The improvement in stability of the triangular silver nanoparticles due to the deposition of chitosan was shown by the lack of aggregation and the detectable redshift of the triangular silver nanoparticles in the in-plane dipolar plasmonic band after p-ATP was added. The triangular silver nanoparticles without chitosan coating, however, immediately aggregated after the addition of p-ATP. Binding of adenine also led to a redshift in the LSPR band.

Joshi et al. investigated the photo-isomerisation of azobenzenes attached on gold nanoprisms with both LSPR and SERS [116]. The photo-reversible cis to trans-

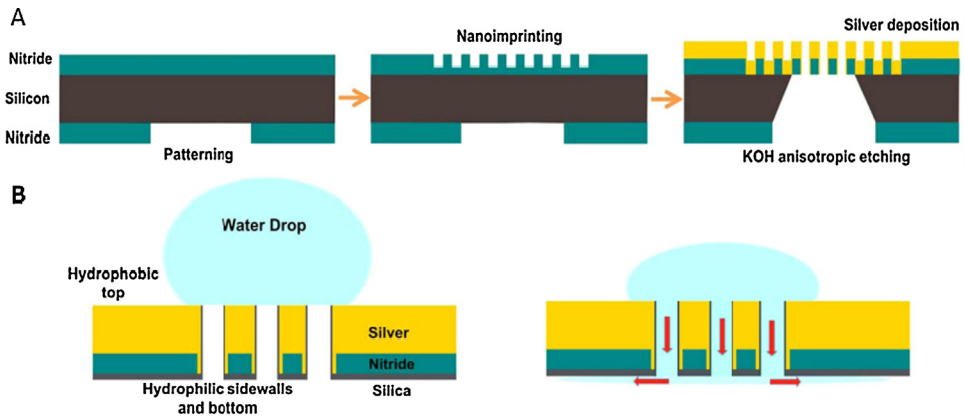

Figure 10 (A) The principal steps of the fabrication of silver nanohole arrays and (B) application of hydrophilic silica on one side for flow through of solution through nanoholes.
Adapted from [114] with permission from American Chemical Society.

isomerisation of attached azobenzene molecules resulted in a 0.6 nm increase in the thickness of the dielectric layer, which was amplified to produce an unprecedented large LSPR wavelength shift of up to 21 nm. Such a large shift was due to the high sensitivity of the nanoprisms to changes in thickness of the local dielectric layer. Plasmonic energy transfer between the nanoprisms and azobenzene molecules also contributed to the LSPR shift. SERS was used to investigate the effect of the azobenzene molecule's conformational change and its photo-reversibility. The SERS intensity of the cis conformation was found to be higher than that of the trans-conformation which could be due to the stronger electromagnetic interaction between the nanoprisms and azobenzene molecules in the cis conformation as the cis isomer is 0.6 nm closer to the surface than the trans-isomer.

Being characteristic of molecules, Raman spectra can serve as fingerprints of many molecules since they originated from a wide range of vibration modes. Unfortunately, the low intensities of Raman signals largely deter Raman spectroscopy to be in biomedicine. The discovery of SERS in the 1970 has offered a good opportunity to significantly enhance the sensitivity of Raman spectroscopy. For SERS fingerprinting, plasmonic nanoparticles and nanostructures are often used because hot spots can be conveniently and reproducibly produced [117]. Recently, Casella et al. presented a silver nanoparticle-based SERS procedure for fingerprinting carotene and haemoglobin in whole blood [118]. Representative SERS features of carotene and haemoglobin were identified. In addition, the oxygenation state of haemoglobin was also identified, demonstrating the potential of fingerprinting biomolecules in a whole blood with no or little sample pre-treatment. In another report, a one-pot synthetic procedure for the preparation of noble metal nanoparticles@mesoporous silica SERS substrate was prepared which was then applied to fingerprint bacteria [119]. On the other hand, SERS was utilised to probe unlabelled nucleic acids with silver nanoparticles as SERS substrates in microfluidic platforms [120]. Micro-molars of nucleic acids in microliters was unambitiously identified. Likewise, a microfluidic platform in conjunction with silver nanoparticles was proposed for sensitive, real-time fingerprint detection of Carbofuran and Alachlor at concentrations as low as 5 ppb [121].

Bioassays utilised plasmonic nanoparticles offer possibilities to improve the sensitivity, opening up new prospects for molecular diagnostics. In all cases, the plasmonic nanoparticles are the most critical component in these assays. Simple and robust synthetic procedures that are capable of reproducibly producing plasmonic nanoparticles with precisely define composition and dimension remain to be fully realised. Although some plasmonic nanoparticles have single-molecule sensitivity, the requirement of sophisticated and bulky instruments primarily limits their applications in centralised laboratories. In this regard, point-of-care applications of plasmonic nanoparticle-based bioassays will probably be dominated by colorimetric methods in the coming years. However, it is expected that automation and the integration of plasmonic nanoparticle-based bioassays with microfluidic platforms and portable optical technologies will eventually revolutionise healthcare industry.

Therapy

Many therapeutic applications of plasmonic nanoparticles have been proposed such as photothermal therapy, photodynamic therapy, drug delivery, diagnosis and even alter gene expression. The following section will review the progress of plasmonic nanoparticles in therapy with representative examples illustrating their operating principles.

Photothermal therapy

Photothermal therapy is the most common application of plasmonic nanoparticles for therapy. Photothermal therapy refers to the irradiation of cells containing plasmonic nanoparticles with near-infrared radiation, whereby the absorbance of such radiation by the plasmonic nanoparticles with surface plasmon resonance in the near-infrared region leads to nanoscale heating of the environment as the oscillations of the nanoparticles decay [122,123]. Such heating is particularly effective for cancer cells due to their increased susceptibility of tumour vascular structures to

increased temperatures of between 40 and 44 °C due to low pH and different environmental conditions of tumour cells, for example low oxygen conditions. Gold nanorods are especially suitable for photothermal therapy due to their tuneable longitudinal plasmon band which is in the near-infrared region [124]. The use of the gold nanorods for photothermal therapy has thus been extensively researched, with the most effective length of the gold nanorods determined [125]. However, photothermal reshaping of the gold nanorods occurs at high temperatures according to the curvature-induced surface diffusion model as reported by Taylor et al. [126]. Experimentally, the gold nanorods with higher aspect ratios were observed to undergo greater extent of reshaping due to their decreased thermodynamic stability, with the gold nanorods of higher aspect ratios reshaping at temperatures below the bulk melting temperature. Research has thus been done to generate alternative nanostructures as well as improve both the photothermal conversion efficiency of the gold nanostructures and the uptake of these gold nanostructures by the cancer cells.

Improving the photothermal conversion efficiency

Two main strategies have been proposed in improving the photothermal conversion efficiency of gold nanostructures: the generation of new nanostructures and the coupling to improve photothermal conversion efficiency.

New nanostructures have been fabricated using unique synthetic methods to improve their photothermal conversion efficiency. Studies have shown that gold nanorods of an appropriate dimension (28 nm × 8 nm) are most effective for plasmonic photothermal therapy amongst individual gold nanoparticles such as nanospheres, nanoshells and nanorods [125,127—131]. Huang et al. further demonstrated that hierarchically assembled of gold nanoparticles allow LSPR to be fine-tuned in the near-infrared (NIR) region for enhanced photothermal conversion efficiency [132]. As shown in Fig. 11, biodegradable poly(ethylene glycol)-b-poly(ε-caprolactone) coated gold nanoparticles are capable of forming nanovesicles (BGV) of densely packed gold nanoparticles which induce strong plasmonic coupling between adjacent gold nanoparticles, thus displaying a photothermal conversion efficiency of 37%. Nonetheless, plasmonic nanostructures with photothermal therapeutic applications have one property in common: they have high near-infrared absorption [133]. This is because human tissues absorb strongly in the visible region but not in the near-infrared region [134]. Having high near-infrared absorption ensures that the plasmonic nanostructures, when injected into the body for treatment, are able to exert their photothermal effect as near-infrared laser radiation can reach the site where the plasmonic nanostructures are, with minimal loss of radiation due to tissue absorption. This was demonstrated by Ye et al. [135] and Huang et al. [136]. The former employed gold nanocrosses which were synthesised by growing along both the ⟨110⟩ and ⟨001⟩ planes. This was done by breaking the face-centred-cubic symmetry of gold nanoparticles through copper-induced formation of single and double twins. The gold nanocrosses exhibited significant near- and mid-IR LSPR, and theoretical simulations revealed that the entire nanocross is excited as long as one of the branches is exposed to incident light, making the nanocrosses ideal for photothermal therapy. The near-IR absorption of the gold nanocrosses led to the efficient photothermal death of cancer cells. Using two-photon fluorescence, the photothermal process was also studied, whereby at 30 s with a laser power of 4.2 W/cm^2, the cell membranes of the cancer cells treated with the gold nanocrosses shrank substantially, eventually collapsed with the gold nanocrosses forming agglomerates. Huang et al. reported the synthesis of a unique gold bellflowers using a liquid-liquid-gas tri-phase system for photoacoustic imaging-guided photothermal therapy [136]. The photothermal conversion efficiency of 74% was much higher for the gold bellflowers than those of other gold nanostructures due to the multi-branched petals which enhanced the local electromagnetic field and the long narrow gaps between the petals that facilitated plasmonic coupling. The photoacoustic signal intensity was also stronger for the gold bellflowers than that of gold nanorods or gold nanostars due to the higher photothermal conversion efficiency of the gold bellflowers and the bell-shaped nanostructure that can amplify photoacoustic signals.

Another strategy is to induce coupling to improve the photothermal efficiency of the gold nanoparticles. This could be done by coupling with other materials, for example reduced graphene oxide as reported by Turcheniuk et al., whereby covalent binding of reduced graphene oxide modified with polyethylene glycol onto gold nanorods enhances their photothermal effect [137]. This was then applied for the specific killing of a uropathogenic strain of *Escherichia coli* at lower power intensities, which can possibly be adopted for the subsequent antibody-free killing of microbes. Plasmonic coupling of gold nanoparticles surface plasmon resonance is another strategy for coupling, causing the absorption peak of the coupled gold nanoparticles to be in the near-infrared region and the near-infrared absorption of the gold nanoparticles to be enhanced. This was demonstrated by Yin et al. with one-dimension chain-like nanostructures made up of gold nanoparticles which were subsequently coated with silica [138]. Their suitability for photothermal therapy was due to their longitudinal plasmonic band at 690 nm, which was in the near-infrared range. Dual plasmonic structures like the gold-Cu_9S_5 structures, investigated by Ding et al., also showed improved nano-heating as compared to Cu_9S_5 structures due to the 50% increase in molar extinction coefficients provided by the gold nanoparticles [139]. With a LSPR band at 1100 nm, the gold-Cu_9S_5 structures offered greater tissue penetration depth than structures with LSPR bands in the infrared region of 700—950 nm. He et al., on the other hand, proposed the synthesis of plasmonic vesicles using amphiphilic block copolymers conjugated on the surface of gold nanoparticles [140]. By adding water, the gold nanoparticles with the amphiphilic block polymers self-assembled into micelle-like structures, resulting in plasmonic coupling and giving strong near-infrared absorption, especially with gold nanoparticles of having a diameter of 40 nm. The strong near-infrared absorption made such vesicle structures useful for photothermal therapy, as shown by the low cell viability of 7.2 ± 3.4% in 4T1 cancer cells incubated with the vesicles and illuminated with a near-infrared laser. In vivo studies in mice with 4T1 tumours showed that tumours treated with

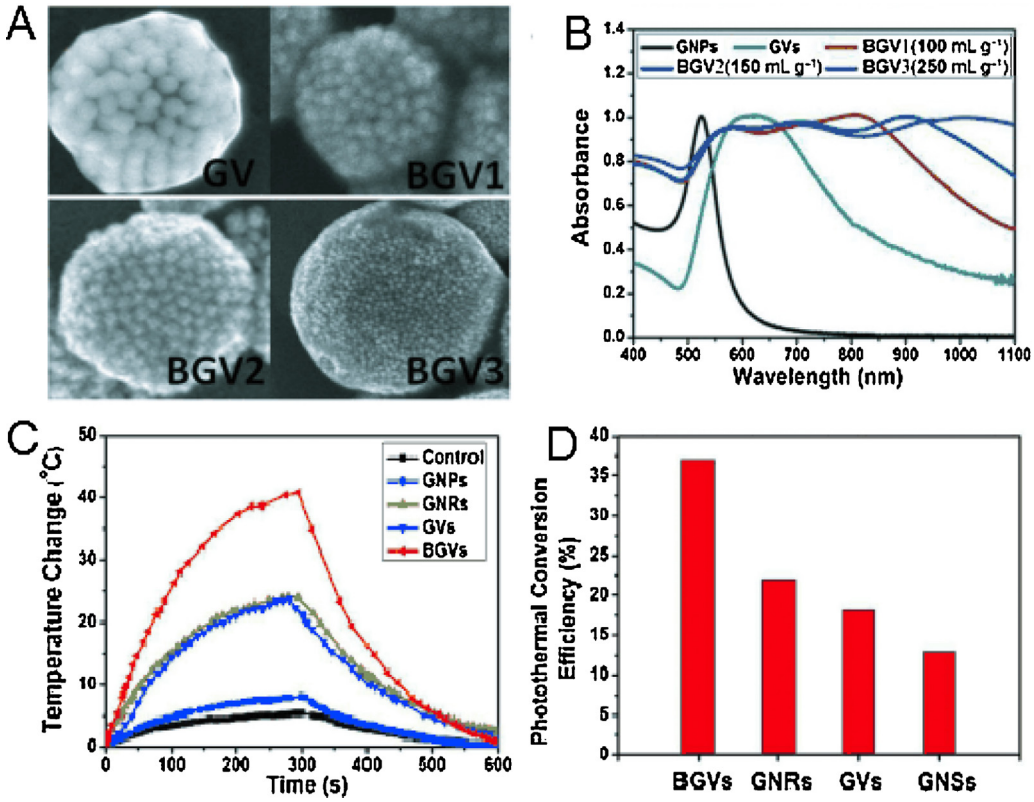

Figure 11 (A) SEM images of gold nanovesicles (GVs), BGV1, BGV2, and BGV3, (B) UV/Vis/NIR spectra of gold nanoparticles (GNPs), GVs, BGVs (the LSPR of BGVs was tuned by varying the GNP concentration), (C) temperature elevation of aqueous solutions of GNPs, gold nanorods (GNRs), GVs and BGVs exposed to laser irradiation (1 W/cm^2) as a function of irradiation time (pure water was used as a negative control) and (D) photothermal conversion efficiencies of BGVs, GVs, GNRs, and gold nanoshells (GNSs). Adapted from [132] with permission from Wiley-VCH.

the vesicles and the near-infrared laser had the tumour completely removed.

Improving uptake of plasmonic nanostructures

Most studies for photothermal applications involve laser irradiation greater than the maximum permissible exposure for skin, which should be avoided under any circumstances. This can be improved with more efficient uptake of the plasmonic nanoparticles, as shown by Mehdizadeh et al. with folate-conjugated gold nanorods [141] or Yuan et al. by the modification of gold nanostars with cell-penetrating peptides [142], specifically the trans-activator of transcription (TAT) peptide from the human immunodeficiency virus type 1. The gold nanostars are also excellent photothermal inducing agents due to their tuneable plasmon band in the near-infrared region, their high absorption-to-scattering ratio and their multiple sharp edges. Thus, both the optimal properties of the gold nanostars as well as the improved cellular uptake of TAT-modified gold nanostars allowed effective photothermal lysis of cancer cells at the lowest reported laser irradiance of 0.2 W/cm^2.

Improving antibacterial properties

Modification of gold nanostructures for improved antibacterial properties was also reported for killing of bacterial cells. This was performed by Fasciani and co-workers with core—shell gold-silver nanostructures stabilised with aspartame, with the gold core serving as an efficient photothermal agent and the silver shells having antibacterial properties like silver nanoparticles [143]. The minimum inhibitory concentration was decreased drastically for the core—shell gold-silver nanostructures stabilised with aspartame as compared to pure gold nanoparticles due to the antibacterial effect of the silver shells. Furthermore, the photothermal activity of the gold-silver nanostructures was demonstrated by the complete killing of the bacterial cells under laser illumination as compared to incomplete killing in the dark. The gold-silver nanostructures were also found to have no effect on the cell viability of human dermal fibroplasts while killing the bacterial cells as compared to the lowering of cell viability by silver nanoparticles due to the release of Ag^+ ions, showing the advantage of the core—shell gold-silver nanostructures over silver nanoparticles as antibacterial agents.

Drug delivery

Plasmonic nanoparticles can also serve as drug carriers. Many mechanisms exist for the employment of plasmonic nanoparticles to assist drug delivery: these have been

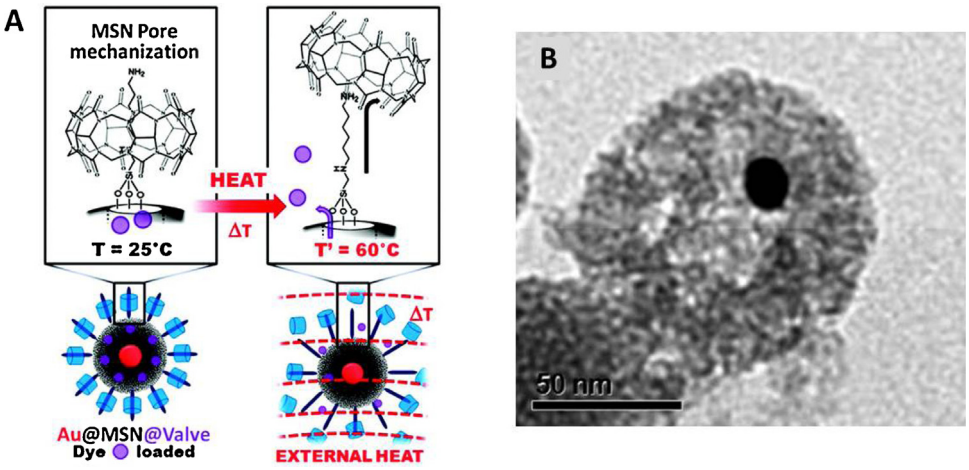

Figure 12 (A) Schematic illustration of the photothermal-heating induced opening of the nano-valves and (B) TEM image of drug release due to laser irradiation at 100 mW.
Adapted from [149] with permission from American Chemical Society.

divided into mechanisms not requiring external stimuli for drug release and mechanisms that only release the drug upon the application of an external stimulus, commonly laser light [144]. In the latter case, both photothermal therapy and drug delivery are often used simultaneously [145].

Mechanisms not requiring external stimuli include drug delivery triggered by a pH change, as reported by Song et al. whereby hollow plasmonic vesicles containing doxorubicin in the core and fabricated with amphiphilic gold nanoparticles released the drug upon encountering acidic pH in the early endosomes or late endosomes/lysosomes [146]. These amphiphilic gold nanoparticles were synthesised by the modification of the gold nanoparticle surface with polyethylene glycol brush, a pH-sensitive polymer and a Raman reporter. SERS signals were used to visualise the assembly and disintegration of the plasmonic vesicles, whereby self-assembly of the plasmonic vesicles occurred at pH 7.4, which exhibited a SERS enhancement factor of 7.2×10^4, while at an acidic pH of 5.0, the plasmonic vesicles were dissolved, resulting in a 34-fold decrease in SERS intensities. Specific endocytosis of the vesicles by breast cancer cells was achieved by attaching the vesicles to an antibody to target the breast cancer cells.

Mechanisms requiring external stimuli often involve the application of laser irradiation, which triggers the photothermal effect of gold nanoparticles, increasing local temperature and releasing the drug. Different mechanisms were developed, most involving the breaking of bonds triggered by the increase in temperature due to the photothermal effect [147—149]. The simplest is the direct conjugation of anticancer drugs onto the surface of the gold nanoparticles, as shown by Xu et al. [147]. Salinomycin was loaded onto the surface of polyelectrolyte-modified gold nanorods through electrostatic adsorption and applied to MCF-7 breast cancer cells for laser-triggered delivery of the drug in cancer stem cells, decreasing the cell viability of cancer stem cells (aldehyde dehydrogenase-positive cells) to zero while total cell viability of both cancer and non-cancer stem cells was at 18%. Such a strategy is promising as by preferentially killing the cancer stem cells, the resistance of cancer stem cells to cancer treatment can be overcome. Intercalation bonds between hairpin DNA and doxorubicin were employed for the targeted delivery of doxorubicin to leukaemia cells as demonstrated by Luo et al. [148]. Gold nanoparticles conjugated to a DNA aptamer for targeting leukaemia cells and a hairpin DNA rich in cytosine and guanine for the attachment of doxorubicin allowed the light-activated drug release due to the gold nanoparticles heating up on the surface when they were irradiated, which melts the hairpin DNA and results in the release of doxorubicin. Croissant et al. proposed the use of non-covalent interactions between a stalk and cucurbituril ring to control pore opening and closing of mesoporous silica nanoparticles containing an anticancer drug [149]. The stalk and the cucurbituril ring formed nano-valves, with the stalk attached to the mesoporous silica nanoparticles (Fig. 12A). The non-covalent interactions between the ammonium groups of the stalk and the carbonyl groups of the cucurbituril ring were activated by a temperature change, whereby the rings stay attached to the stalk at 25 °C, which closes the pores, but they were removed from the stalk at 60 °C, causing the pores to be opened and hence drug to be released (Fig. 12B). Such a temperature change was activated by near-infrared laser, which caused the heating of the environment due to the photothermal effect of the gold nanoparticles embedded in the silica nanoparticles.

To enhance the effect of drug delivery by the plasmonic nanoparticles, another strategy has also been developed: to employ the body's inbuilt mechanisms for enhancing drug delivery. This is a novel way of enhancing drug delivery without the need for complicated mechanisms to ensure light-triggered drug delivery. On the other hand, body mechanisms vary from person to person, and thus could be less reliable. One of such mechanisms is the use of endocytosis, as elegantly demonstrated by Lukianova-Hleb [150]. Plasmonic nano-bubbles were formed due to the strong absorption of light by the LSPR of the plasmonic nanoparticles. As a result of the LSPR decay, temperatures of the water medium around the gold nanoparticles increase,

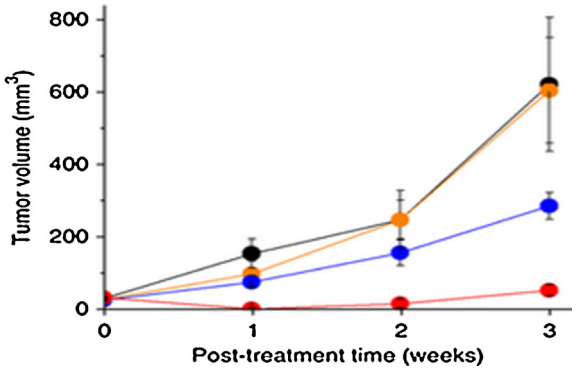

Figure 13 Tumour volume in mice treated with all four treatments (red), with chemoradiation (blue), plasmonic nanobubbles alone (orange) and control (black).
Adapted from [150] with permission from Nature Publishing Group.

causing superheating and generating vapour-bubbles. This results in rupturing of the cell or co-localised liposomes. By targeting both gold nanoparticles and liposomes containing either doxorubicin or paclitaxel in cancer cells and achieving co-localisation of the gold nanoparticles and drug-loaded liposomes by receptor-mediated endocytosis, either rupturing of the cell by the photothermal effect or rupturing of drug-loaded liposomes occurs when cancer cells were illuminated with a laser. This effect is further enhanced by clustering of the gold nanoparticles, which causes plasmonic coupling. Also, by applying X-ray at the site of drug delivery, amplification of X-ray by the gold nanoparticle clusters at the site of drug release also increases the efficiency of the drug. The synergism of these four effects, the encapsulated drug in the liposome, the X-ray amplification, the near-infrared laser pulse and the colloidal gold nanoparticles, resulted in a 17-fold increase in the therapeutic effect on highly aggressive cancer cells after a single administration after a week as compared to chemo-radiation (Fig. 13). Wang et al. elucidated the effect of highly localised heat generated by the plasmonic nanoparticles, specifically silica-coated gold nanorods, on drug-resistant cancer cells, specifically doxorubicin-resistant cells [151]. Hyperthermia of doxorubicin-resistant cells increased their sensitivity to doxorubicin, decreasing the concentration of doxorubicin required to halve their population from 158 μM to 12.7 μM. Its mechanism can be explained as such: highly localised heat is generated upon radiation by the gold nanorods. Doxorubicin-resistant cells, which normally induce an efflux of doxorubicin through Pgp proteins, were observed to increase doxorubicin uptake of up to 8-fold in 12 h. This was found to be due to firstly the trigger in the heat shock factor trimers production, which competes with the transcription factor of the pathway for the synthesis of Pgp, leading to decreased Pgp production and thus decreased export. Also, mutant p53 levels were decreased due to the photothermal treatment, leading to increased susceptibility of the doxorubicin-resistant cells to apoptosis as the anti-apoptotic activity of mutant p53 was decreased.

Diagnosis of cancer

Diagnosis of cancer and photothermal therapy can also be performed simultaneously using Raman signals, as shown by Yang et al. with gold-silver core—shell structures [152], Chen et al. with gold nanorattles [153] and Nergiz et al. with graphene oxide modified-gold nanostars [154]. The gold nanorattles used were hollow nanoparticles with gold nanoparticle cores coated with Raman reporter middle shells and then outer shells made of gold. The gold nanorattles were then covalently conjugated to an antibody targeting the estrogen receptor for internalisation as estrogen receptors were overexpressed on the surface of breast cancer cells. This gave strong SERS signals for internalised gold nanorattles as shown by transmission electron microscopy, allowing for the identification of breast cancer cells. More extensive cellular damage was also observed for cells incubated with the gold nanorattles modified with the antibody rather than gold nanorattles that had polyethylene glycol on their surface upon laser radiation, showing that the antibody-modified gold nanorattles were effective in photothermal treatment of the cancer cells. Nergiz et al. took this one step further by omitting the need for a Raman reporter with graphene oxide-modified gold nanostars, with the graphene oxide offering intrinsic Raman detection, increased stability of the plasmonic composite as well as internalisation of the gold nanostars by epithelial breast cancer cells, thus allowing for simultaneous diagnosis and photothermal therapy of cancer cells [154].

Altering gene expression

The photothermal therapeutic effect of plasmonic nanoparticles can not only be used for killing cancer cells, but also for the modification of gene expression in cells as demonstrated by Kalies et al. [155] and Martin-Saavedra et al. [156]. Martin-Saavedra et al. reported the incorporation of hollow gold nanostructures into fibrin hydrogels for the patterning of transgene expression in cells [156]. The patterning of transgene expression was both demonstrated in in vitro assays with mice cells and in vivo assays within the mice. This was performed by first genetically modifying cells by the addition of a firefly luciferase gene conjugated to a heat-activated, dimeriser-dependent gene switch and then adding the fibrin hydrogels containing the hollow gold nanoparticles. These cells were then treated with rapamycin to trigger dimerisation and near-infrared irradiation to heat up the cells. Bio-fluorescence was then observed at the location of the near-infrared radiation. Furthermore, by re-administering rapamycin and applying near-infrared radiation again, bio-fluorescence was again observed. The potential for patterned transgene expression demonstrated in this article opens up possibilities for triggering transgene expression at the site required for therapy.

Photodynamic therapy

Photodynamic therapy, unlike photothermal therapy, triggers the generation of reactive oxygen species to kill cells, in particular cancer cells [157]. Photodynamic therapy can be performed with the coupling of photo-sensitisers with

plasmonic nanoparticles as demonstrated by Fales et al. with a cell-penetrating peptide, TAT, to modify gold nanostars for enhanced photodynamic effects and increased enhancement of Raman signals [158], and Shi et al. with photosensitiser-attached gold nanorods for the specific photodynamic therapy of cancer cells [159]. Photo-sensitisers convert dioxygen into singlet oxygen upon irradiation. As investigated by Shi and co-workers [159], AlPcS4, the photosensitiser, attached to the gold nanorods is close enough to the gold nanorods such that the AlPcS4 conjugated to the gold nanorods were non-phototoxic as their close proximity to the gold nanorods entails transmission of energy from the photo-sensitisers to the gold nanorods. With near-infrared radiation however, the AlPcS4 was released. A high power density coupled with low power density mode was adopted because such an approach allowed for the specific killing of cells containing the gold nanorod-AlPcS4 conjugate as the initial short duration of high power density laser allows for speeding up of the release of AlPcS4 from the gold nanorods while the subsequent low power allows for prolonged photodynamic therapeutic effects through the gradual release of AlPcS4. Cell viability, however, remained high for normal cells which take up free AlPcS4 due to insufficient laser power and low cellular concentrations, leading to specific death of cancer cells containing gold nanorod-AlPcS4 conjugates.

Photodynamic therapy of cancer cells can also be performed without photosensitizers as shown by Kumar et al. with gold core-petal nanoparticles, which were generated through the Au(III)-induced oxidation of the catechol groups on polydopamine which was homogeneously assembled on the surface of gold nanoparticles [160]. Partial removal of the polydopamine layer on the gold nanoparticles causes preferential growth along the petal nanostructures. Such core-petal nanoparticles were found to have both photothermal effects, as shown from its high photothermal conversion efficiency of 32%, and high photodynamic effect, as shown from the large generation of singlet oxygen as compared to gold nanoparticles. This indicated that the petal length and density is essential for singlet oxygen production. An increase in the number of protruding petals was found to decrease cell viability as shown by nanoparticles with the greatest number of and longest petals, which killed nearly all cells despite an increase in temperature only until 42 °C. The percentage contribution of reactive oxygen species in causing cell death was found to be 88% as measured by the addition of ascorbic acid, an anti-oxidant, while the remaining 12% was due to photothermal effects.

The rapid progress of therapeutic applications of plasmonic nanoparticles has offered ample opportunities in biomedicine. However, besides the obvious benefits brought about by plasmonic nanoparticles, their pharmacokinetics, pharmacodynamics, toxicity and ultimate fate in biological systems remains poorly understood. Recent studies have indicated that plasmonic nanoparticles could dramatically affect epigenetic processes [161—163]. For example, gold nanoparticles were found to significantly alter both gene [161] and microRNA expressions [163]. Mouse foetal lung and liver have significantly up-regulated miR-183 after exposure to gold nanoparticles and up-regulated miR-183 expression was found to be close associated with lung cancer incidence [164]. It is therefore vital to thoroughly assess their adverse effects before proceeding with clinical trials.

Conclusion and prospects

In this article, the plasmonic properties of nanostructures and nanoparticles have been shown to give rise to a wide range of phenomena, including but not limited to metal-enhanced fluorescence, SPR, SERS and photothermal and photodynamic properties. In particular, an overarching theme of plasmonic coupling has been a strategy in bioassays and therapy, for the enhancement of these effects. Each of those phenomena has its own strengths and weaknesses, with the colourimetric method of detection using localised surface plasmon resonance easily constructed and detectable with the naked eye. However, sensing using surface plasmon resonance usually has a lower sensitivity than metal-enhanced fluorescence and SERS due to some degree of the non-specific nature of surface plasmon resonance sensing. SERS allows for the molecular identification of bioanalytes, which fluorescence and surface plasmon resonance do not provide for. This article has also shown the application of the phenomena to biomedical applications such as bioassays and therapy. However, much still needs to be done to improve the speed and accuracy as well as lowering the cost of such bioassays. Even though single nanoparticle bioassays have already been reported, their sensitivity can be further increased by the control of their shape, size and surface chemistry. Single nanoparticle bioassays can also be applied for the sensing of a wider range of bioanalytes or even tip-enhanced Raman scattering, allowing for bio-analyte identification. Also, for successful application of the plasmonic nanoparticles in therapeutic applications, the distribution and long-term toxic effect of the plasmonic nanoparticles must be thoroughly evaluated since most of the metal plasmonic nanoparticles like gold and silver are fairly stable and non-biodegradable. The elimination of such plasmonic nanoparticles when applied for biosensing purposes must also be carefully studied. The development of non-metal and biodegradable plasmonic materials may offer an attractive alternative [144]. Nevertheless, the potential of the plasmonic properties of nanoparticles in improving sensitivities of bioassays and cancer therapy efficiency suggests that the field of the plasmonic nanoparticles for biomedical applications remains promising.

Acknowledgement

This work is supported by Ministry of Education.

References

[1] R. Wilsona, Chem. Soc. Rev. 37 (2008) 2028.
[2] S. Roy, Z.Q. Gao, Nano Today 4 (2009) 318.
[3] E. Boisseliera, D. Astruc, Chem. Soc. Rev. 38 (2009) 1759.
[4] M. Larguinho, P.V. Baptista, J. Proteomics 75 (2012) 2811.
[5] B. Smolkova, N.E. Yamani, A.R. Collins, A.C. Gutleb, M. Dusinska, Food Chem. Toxicol. 77 (2015) 64.
[6] C.J. Murphy, A.M. Gole, J.W. Stone, P.N. Sisco, A.M. Alkilany, E.C. Goldsmith, et al., Acc. Chem. Res. 41 (2008) 1721.

[7] F.J.G. de Abajo, Nature 483 (2012) 417.
[8] S.K. Ghosh, T. Pal, Chem. Rev. 107 (2007) 4797.
[9] S.T. Kochuveedu, D.H. Kim, Nanoscale 6 (2014) 4966.
[10] M. Fleischmann, P.J. Hendra, A. McQuillan, J. Chem. Phys. Lett. 26 (1974) 163.
[11] J. Olson, S. Dominguez-Medina, A. Hoggard, L.Y. Wang, W.S. Chang, S. Link, Chem. Soc. Rev. 44 (2015) 40.
[12] J. Tang, R.A. Marcus, J. Chem. Phys. 123 (2005) 054704.
[13] C. Eggeling, J. Widengren, R. Rigler, C.A.M. Seidel, Anal. Chem. 70 (1998) 2651.
[14] D. Jaque, L.M. Maestro, B. del Rosal, P. Haro-Gonzalez, A. Benayas, J.L. Plaza, et al., Nanoscale 6 (2014) 9494.
[15] P.K. Jain, X.H. Huang, I.H. El-Sayed, M.A. El-Sayed, Acc. Chem. Res. 41 (2008) 1578.
[16] J. Zhao, A.O. Pinchuk, J.M. McMahon, S. Li, L.K. Ausman, A.L. Atkinson, et al., Acc. Chem. Res. 41 (2008) 1710.
[17] N.C. Tansil, Z.Q. Gao, Nano Today 1 (2006) 28.
[18] K. Aslan, C.D. Geddes, in: C.D. Geddes (Ed.), Metal-Enhanced Fluorescence: Progress Towards a Unified Plasmon-Fluorophore Description, John Wiley & Sons, New York, 2010.
[19] C.D. Geddes, J.R. Lakowicz, J. Fluoresc. 12 (2002) 121.
[20] J.R. Lakowicz, Anal. Biochem. 337 (2005) 171.
[21] H. Mishra, B.L. Mali, J. Karolin, A.I. Dragan, C.D. Geddes, Phys. Chem. Chem. Phys. 15 (2013) 19538.
[22] Z. Zhou, H. Huang, Y. Chen, F. Liu, C.Z. Huang, N. Li, Biosens. Bioelectron. 52 (2014) 367.
[23] A.I. Dragan, E.S. Bishop, J.R. Casas-Finet, R.J. Strouse, J. McGivney, M.A. Schenerman, et al., Plasmonics 7 (2012) 739.
[24] J. Zhang, J.R. Lakowicz, J. Phys. Chem. B 110 (2006) 2387.
[25] J. Geng, J. Liang, Y. Wang, G.G. Gurzadyan, B. Liu, J. Phys. Chem. B 115 (2011) 3281.
[26] X. Wang, F. He, X. Zhu, F. Tang, L. Li, Sci. Rep. 4 (2014) 4406.
[27] N. Akbay, J.R. Lakowicz, K. Ray, J. Phys. Chem. C 116 (2012) 10766.
[28] A.V. Sorokin, A.A. Zabolotskii, N.V. Pereverzev, I.I. Bespalova, S.L. Yefimova, Y.V. Malyukin, et al., J. Phys. Chem. C 119 (2015) 2743.
[29] Y.S. Chi, H.R. Byon, B.S. Lee, B. Kong, H.C. Choi, I.S. Choi, Adv. Funct. Mater. 18 (2008) 3395.
[30] K. Wang, J. Liao, X. Yang, M. Zhao, M. Chen, W. Yao, Biosens. Bioelectron. 63 (2015) 172.
[31] M. Ganguly, J. Pal, C. Mondal, A. Pal, T. Pal, Chem. Eur. J. 20 (2014) 12470.
[32] K. Aslan, I. Gryczynski, J. Malicka, E. Matveeva, J.R. Lakowicz, C.D. Geddes, Curr. Opin. Biotechnol. 16 (2005) 55.
[33] G. Hong, S.M. Tabakman, K. Welsher, H. Wang, X. Wang, H. Dai, J. Am. Chem. Soc. 132 (2010) 15920.
[34] H.I. Peng, C.M. Strohsahl, K.E. Leach, T.D. Krauss, B.L. Miller, ACS Nano 3 (2009) 2265.
[35] Q. Li, C. Cui, D.A. Higgins, J. Li, J. Am. Chem. Soc. 134 (2012) 14467.
[36] F. Degliangeli, P. Kshirsagar, V. Brunetti, P.P. Pompa, R. Fiammengo, J. Am. Chem. Soc. 136 (2014) 2264.
[37] L. Zhou, F. Ding, H. Chen, W. Ding, W. Zhang, S.Y. Chou, Anal. Chem. 84 (2012) 4489.
[38] J. Lee, S. Lee, M. Jen, Y. Pang, J. Phys. Chem. C 119 (2015) 23285.
[39] B.K. Gorityala, Z. Lu, M.L. Leow, J. Ma, X.W. Liu, J. Am. Chem. Soc. 134 (2012) 15229.
[40] J. Lee, S.R. Ahmed, S. Oh, J. Kim, T. Suzuki, K. Parmar, et al., Biosens. Bioelectron. 64 (2015) 311.
[41] S.H. Cao, Z.X. Zou, Y.H. Weng, W.P. Cai, Q. Liu, Y.Q. Li, Biosens. Bioelectron. 58 (2014) 258.
[42] S.H. Cao, W.P. Cai, Q. Liu, K.X. Xie, Y.H. Weng, Y.Q. Li, Chem. Commun. 50 (2014) 518.
[43] S.H. Cao, W.P. Cai, Q. Liu, K.X. Xie, Y.H. Weng, S.X. Huo, et al., J. Am. Chem. Soc. 136 (2014) 6802.
[44] W. Deng, D. Jin, K. Drozdowicz-Tomsia, J. Yuan, J. Wu, E.M. Goldys, Adv. Mater. 23 (2011) 4649.
[45] K. Tawa, M. Umetsu, H. Nakazawa, T. Hattori, I. Kumagai, ACS Appl. Mater. Interfaces 5 (2013) 8628.
[46] M.H. Chowdhury, K. Ray, S.K. Gray, J. Pond, J.R. Lakowicz, Anal. Chem. 81 (2009) 1397.
[47] M.H. Chowdhury, S. Chakraborty, J.R. Lakowicz, K. Ray, J. Phys. Chem. C 115 (2011) 16879.
[48] M.H. Chowdhury, K. Ray, K. Aslan, J.R. Lakowicz, C.D. Geddes, J. Phys. Chem. C 111 (2007) 18856.
[49] W. Deng, K. Drozdowicz-Tomsia, D. Jin, E.M. Goldys, Anal. Chem. 81 (2009) 7248.
[50] H. Szmacinski, R. Badugu, J.R. Lakowicz, J. Phys. Chem. C 114 (2010) 21142.
[51] S. Zeng, D. Baillargeat, H. Ho, K. Yong, Chem. Soc. Rev. 43 (2014) 3426.
[52] R.H. Ritchie, Phys. Rev. 106 (1957) 874.
[53] H. Reather, Surface Polaritons on Smooth and Rough Surfaces and on Gratings, Springer-Verlag, Berlin, 1988.
[54] F.J. Garcia-Vidal, J.B. Pendry, Phys. Rev. Lett. 77 (1996) 1163.
[55] A.D. McFarland, R.P. Van Duyne, Nano Lett. 3 (2003) 1057.
[56] T.R. Jensen, G.C. Schatz, R.P. Van Duyne, J. Phys. Chem. B 103 (1999) 2394.
[57] J. Homola, Chem. Rev. 108 (2008) 462.
[58] K.A. Willets, R.P. Van Duyne, Annu. Rev. Phys. Chem. 58 (2007) 267.
[59] C.C. Yu, K.H. Ho, H.L. Chen, S.Y. Chuang, S.C. Tseng, W.F. Su, Biosens. Bioelectron. 33 (2012) 267.
[60] J. Feng, V.S. Siu, A. Roelke, V. Mehta, S.Y. Rhieu, G.T. Palmore, et al., Nano Lett. 12 (2012) 602.
[61] S. Zuccon, P. Zuppella, M. Cristofani, S. Silvestrini, A.J. Corso, M. Maggini, M.G. Pelizzo, J. Opt. 16 (2014) 55001.
[62] W. Law, K. Yong, A. Baev, P.N. Prasad, ACS Nano 5 (2011) 4858.
[63] L. Niu, K. Cheng, Y. Wu, T. Wang, Q. Shi, D. Liu, et al., Biosens. Bioelectron. 50 (2013) 137.
[64] H. Im, H. Shao, Y.I. Park, V.M. Peterson, C.M. Castro, R. Weissleder, et al., Nat. Biotechnol. 32 (2014) 490.
[65] Y. Oh, W. Lee, Y. Kim, D. Kim, Biosens. Bioelectron. 51 (2014) 401.
[66] M. Toma, K. Cho, J.B. Wood, R.M. Corn, Plasmonics 9 (2013) 765.
[67] A.A. Jamali, B. Witzigmann, Plasmonics 9 (2014) 1265.
[68] L. Sun, Q. Li, W. Tang, J. Di, Y. Wu, Microchim. Acta 181 (2014) 1991.
[69] P. Dong, Y. Wu, W. Guo, J. Di, Plasmonics 8 (2013) 1577.
[70] W.P. Hall, J. Modica, J. Anker, Y. Lin, M. Mrksich, R.P. Van Duyne, Nano Lett. 11 (2011) 1098.
[71] G.K. Joshi, S. Deitz-McElyea, M. Johnson, S. Mali, M. Korc, R. Sardar, Nano Lett. 14 (2014) 6955.
[72] Y. Shen, J. Zhou, T. Liu, Y. Tao, R. Jiang, M. Liu, et al., Nat. Commun. 4 (2013) 2381.
[73] K.M. Mayer, J.H. Hafner, Chem. Rev. 111 (2011) 3828.
[74] L. Tian, K.-K. Liu, J.J. Morrissey, N. Gandra, E.D. Kharasch, S. Singamaneni, J. Mater. Chem. B 2 (2014) 167.
[75] Y. Choi, J.-H. Choi, L. Liu, B.-K. Oh, S. Park, Chem. Mater. 25 (2013) 919.
[76] D. Seo, G. Park, H. Song, J. Am. Chem. Soc. 134 (2012) 1221.
[77] Y. Hu, L. Zhang, Y. Zhang, B. Wang, Y. Wang, Q. Fan, et al., ACS Appl. Mater. Interfaces 7 (2015) 2459.
[78] Y. Liu, W. Fang, Z. Wu, G. Zhou, W. Yi, X. Zhou, et al., Talanta 128 (2014) 305.
[79] S. Unser, I. Campbell, D. Jana, L. Sagle, Analyst 140 (2014) 590.
[80] A. Vanderkooy, Y. Chen, F. Gonzaga, M.A. Brook, ACS Appl. Mater. Interfaces 3 (2011) 3942.
[81] X.M. Nie, R. Huang, C.X. Dong, L.J. Tang, R. Gui, J.H. Jiang, Biosens. Bioelectron. 58 (2014) 314.

[82] R. de la Rica, M.M. Stevens, Nat. Nanotechnol. 7 (2012) 821.
[83] A. Niazov-Elkan, E. Golub, E. Sharon, D. Balogh, I. Willner, Small 10 (2014) 2883.
[84] J. Wang, J. Lu, S. Su, J. Gao, Q. Huang, L. Wang, et al., Biosens. Bioelectron. 65 (2014) 171.
[85] L. Guo, Y. Xu, A.R. Ferhan, G. Chen, D.H. Kim, J. Am. Chem. Soc. 135 (2013) 12338.
[86] N. Jornet-Martinez, M. Gonzalez-Bejar, Y. Moliner-Martinez, P. Campins-Falco, J. Perez-Prieto, Anal. Chem. 86 (2014) 1347.
[87] W. Shen, H.M. Deng, A.K.L. Teo, Z.Q. Gao, Chem. Commun. 48 (2012) 10225.
[88] W. Shen, H.M. Deng, Z.Q. Gao, J. Am. Chem. Soc. 134 (2012) 14678.
[89] X.J. Yang, Y.B. Yu, Z.Q. Gao, ACS Nano 8 (2014) 4902.
[90] B. Malile, J.I. Chen, J. Am. Chem. Soc. 135 (2013) 16042.
[91] J.H. Oh, B.C. Kim, J.S. Lee, Anal. Bioanal. Chem. 406 (2014) 7591.
[92] X.J. Yang, Y.Q. Ren, Z.Q. Gao, Chem. Eur. J. 21 (2015) 988.
[93] C.H. Zhou, J.Y. Zhao, D.W. Pang, Z.L. Zhang, Anal. Chem. 86 (2014) 2752.
[94] X.J. Yang, Z.Q. Gao, Chem. Commun. 51 (2015) 6928.
[95] L. Rodriguez-Lorenzo, R. de la Rica, R.A. Alvarez-Puebla, L.M. Liz-Marzan, M.M. Stevens, Nat. Mater. 11 (2012) 604.
[96] H. Sadabadi, S. Badilescu, M. Packirisamy, R. Wuthrich, Biosens. Bioelectron. 44 (2013) 77.
[97] S. Balamurugan, K.M. Mayer, S. Lee, S.A. Soper, J.H. Hafner, D.A. Spivak, J. Mol. Recogn. 26 (2013) 402.
[98] A. Abbas, L. Tian, J.J. Morrissey, E.D. Kharasch, S. Singamaneni, Adv. Funct. Mater. 23 (2013) 1789.
[99] G. Raschke, S. Kowarik, T. Franzl, C. So1nnichsen, T.A. Klar, J. Feldmann, et al., Nano Lett. 3 (2003) 935.
[100] L. Qin, Y. Li, D. Li, C. Jing, B. Chen, W. Ma, et al., Angew. Chem. Int. Ed. 51 (2012) 140.
[101] M.N. Bui, S. Ahmed, A. Abbas, Nano Lett. 15 (2015) 6239.
[102] L. Zhang, Y. Zhang, Y. Hu, Q. Fan, W. Yang, A. Li, et al., Chem. Commun. 51 (2015) 294.
[103] I. Ament, J. Prasad, A. Henkel, S. Schmachtel, C. Sönnichsen, Nano Lett. 12 (2012) 1092.
[104] J. Chen, G. Qin, J. Wang, J. Yu, B. Shen, S. Li, et al., Biosens. Bioelectron. 44 (2013) 191.
[105] R.W. Taylor, T. Lee, O.A. Scherman, R. Esteban, J. Aizpurua, F.M. Huang, et al., ACS Nano 5 (2011) 3878.
[106] J. Song, B. Duan, C. Wang, J. Zhou, L. Pu, Z. Fang, et al., J. Am. Chem. Soc. 136 (2014) 6838.
[107] X. Qian, X. Zhou, S. Nie, J. Am. Chem. Soc. 130 (2008) 14934.
[108] M. Li, S.K. Cushing, H. Liang, S. Suri, D. Ma, N. Wu, Anal. Chem. 85 (2013) 2072.
[109] M. Li, S.K. Cushing, J. Zhang, S. Suri, R. Evans, D. Ma, et al., ACS Nano 7 (2013) 4967.
[110] M.J. Mulvihill, X.Y. Ling, J. Henzie, P. Yang, J. Am. Chem. Soc. 138 (2010) 268.
[111] X. Qian, J. Li, S. Nie, J. Am. Chem. Soc. 131 (2009) 7540.
[112] L. Fabris, M. Dante, G. Braun, S.J. Lee, N.O. Reich, M. Moskovits, J. Am. Chem. Soc. 129 (2007) 6086.
[113] Y.J. Oh, K.H. Jeong, Lab Chip 14 (2014) 865.
[114] S. Kumar, S. Cherukulappurath, T.W. Johnson, S.-H. Oh, Chem. Mater. 26 (2014) 6523.
[115] M. Potara, A.-M. Gabudean, S.J. Astilean, Mater. Chem. 21 (2011) 3625.
[116] G.K. Joshi, K.N. Blodgett, B.B. Muhoberac, M.A. Johnson, K.A. Smith, R. Sardar, Nano Lett. 14 (2014) 532.
[117] K. Kneipp, M. Moskovits, H. Kneipp, Surface-Enhanced Raman Scattering — Physics and. Applications, in: Topics Appl. Phys., vol. 103, Springer, New York, 2006.
[118] M. Casella, A. Lucotti, M. Tommasini, M. Bedonic, E. Forvic, F. Gramaticac, et al., Spectrochim. Acta A 79 (2011) 915.
[119] C. Lin, C. Yu, Y. Yang, Y. Chu, H. Lin, H. Chang, NEMS (2009) 249.
[120] E. Prado, A. Colin, L. Servant, S. Lecomte, J. Phys. Chem. C 118 (2014) 13965.
[121] J. Parisi, Q. Dong, Y. Lei, RSC Adv. 5 (2015) 14081.
[122] F. Jabeen, M. Najam-ul-Haq, R. Javeed, C.W. Huck, G.K. Bonn, Molecules 19 (2014) 20580.
[123] S. Hwang, J. Nam, S. Jung, J. Song, H.S. Doh, et al., Nanomedicine 9 (2014) 2003.
[124] K. Xia, L.M. Zhang, Y.F. Huang, Z.X. Lu, J. Nanosci. Nanotechnol. 15 (2015) 63.
[125] M.A. Mackey, M.R. Ali, L.A. Austin, R.D. Near, M.A. El-Sayed, J. Phys. Chem. B 118 (2014) 1319.
[126] A.B. Taylor, A.M. Siddiquee, J.W.M. Chon, ACS Nano 8 (2014) 12071.
[127] G. von Maltzahn, J. Park, A. Agrawal, N.K. Bandaru, S.K. Das, M.J. Sailor, et al., Cancer Res. 69 (2009) 3893.
[128] C.H. Loo, A. Lin, L.R. Hirsch, M.H. Lee, J.J. Barton, et al., Technol. Cancer Res. Treat. 3 (2004) 33.
[129] X. Huang, I.H. El-Sayed, M.A. El-Sayed, J. Am. Chem. Soc. 128 (2006) 2115.
[130] M. Hu, H. Petrova, J. Chen, J.M. McLellan, A.R. Siekkinen, M. Marquez, et al., J. Phys. Chem. B 110 (2006) 1520.
[131] G. Park, H. Kwon, D.W. Kwak, S.Y. Park, M. Kim, J. Lee, Nano Lett. 12 (2012) 1638.
[132] P. Huang, J. Lin, W. Li, P. Rong, Z. Wang, et al., Angew. Chem. Int. Ed. 52 (2013) 13958.
[133] X. Huang, P.K. Jain, I.H. El-Sayed, M.A. El-Sayed, Lasers Med. Sci. 23 (2008) 217.
[134] A.M. Smith, M.C. Mancini, S. Nie, Nat. Nanotechnol. 4 (2009) 710.
[135] E. Ye, K.Y. Win, H.R. Tan, M. Lin, C.P. Teng, A. Mlayah, J. Am. Chem. Soc. 133 (2011) 8506.
[136] P. Huang, P. Rong, J. Lin, W. Li, X. Yan, M.G. Zhang, J. Am. Chem. Soc. 136 (2014) 8307.
[137] K. Turcheniuk, C.-H. Hage, J. Spadavecchia, A.Y. Serrano, I. Larroulet, A. Pesquera, et al., J. Mater. Chem. B 3 (2015) 375.
[138] Z. Yin, W. Zhang, Q. Fu, H. Yue, W. Wei, P. Tang, et al., Small 10 (2014) 3619.
[139] X. Ding, C.H. Liow, M. Zhang, R. Huang, C. Li, H. Shen, et al., J. Am. Chem. Soc. 136 (2014) 15684.
[140] J. He, X. Huang, Y.C. Li, Y. Liu, T. Babu, M.A. Aronova, et al., J. Am. Chem. Soc. 135 (2013) 7974.
[141] A. Mehdizadeh, S. Pandesh, A. Shakeri-Zadeh, S.K. Kamrava, M. Habib-Agahi, M. Farhadi, et al., Lasers Med. Sci. 29 (2014) 939.
[142] H. Yuan, A.M. Fales, T. Vo-Dinh, J. Am. Chem. Soc. 134 (2012) 11358.
[143] C. Fasciani, M.J. Silvero, M.A. Anghel, G.A. Arguello, M.C. Becerra, J.C. Scaiano, J. Am. Chem. Soc. 136 (2014) 17394.
[144] J.B. Song, P. Huang, H.W. Duan, X.Y. Chen, Acc. Chem. Res. 48 (2015) 2506.
[145] J. Song, X. Yang, O. Jacobson, L. Lin, P. Huang, G. Niu, et al., ACS Nano 2015 (9) (2015) 9199.
[146] J. Song, J. Zhou, H. Duan, J. Am. Chem. Soc. 134 (2012) 13458.
[147] Y. Xu, J. Wang, X. Li, Y. Liu, L. Dai, X. Wu, et al., Biomaterials 35 (2014) 4667.
[148] Y. Luo, Y. Shiao, Y. Huang, ACS Nano 5 (2011) 7796.
[149] J. Croissant, J.I. Zink, J. Am. Chem. Soc. 134 (2012) 7628.
[150] E.Y. Lukianova-Hleb, X. Ren, R.R. Sawant, X. Wu, V.P. Torchilin, D.O. Lapotko, Nat. Med. 20 (2014) 778.
[151] L. Wang, X. Lin, J. Wang, Z. Hu, Y. Ji, S. Hou, et al., Adv. Funct. Mater. 24 (2014) 4229.
[152] J. Yang, D. Shen, L. Zhou, W. Li, J. Fan, A.M. El-Toni, et al., Adv. Health Mater. 3 (2014) 1620.

[153] Z. Chen, D. Yu, Y. Huang, Z. Zhang, T. Liu, J. Zhan, Sci. Rep. 4 (2014) 6709.
[154] S.Z. Nergiz, N. Gandra, S. Tadepalli, S. Singamaneni, ACS Appl. Mater. Interfaces 6 (2014) 16395.
[155] S. Kalies, D. Heinemann, M. Schomaker, H.M. Escobar, A. Heisterkamp, T. Ripken, et al., J. Biophotonics 7 (2014) 825.
[156] F.M. Martin-Saavedra, V. Cebrian, L. Gomez, D. Lopez, M. Arruebo, C.G. Wilson, et al., Biomaterials 35 (2014) 8134.
[157] D.E. Dolmans, D. Fukumura, R.K. Jain, Nat. Rev. Cancer 3 (2003) 380.
[158] A.M. Fales, H. Yuan, T. Vo-Dinh, Mol. Pharm. 10 (2013) 2291.
[159] Z. Shi, W. Ren, A. Gong, X. Zhao, Y. Zou, E.M. Brown, et al., Biomaterials 35 (2014) 7058.
[160] A. Kumar, S. Kumar, W.K. Rhim, G.H. Kim, J.M. Nam, J. Am. Chem. Soc. 136 (2014) 16317.
[161] C.T. Ng, S.T. Dheen, W.C. Yip, C.N. Ong, B.H. Bay, L.Y.L. Yung, Biomaterials 32 (2011) 7609.
[162] A. Mazumder, G.V. Shivashankar, Biophys. J. 93 (2007) 2209.
[163] R. Balansky, M. Longobardi, G. Ganchev, M. Iltcheva, N. Nedyalkov, P. Atanasov, Mutat. Res. 751 (2013) 42.
[164] U. Võsa, T. Vooder, R. Kolde, J. Vilo, A. Metspalu, T. Annilo, Int. J. Cancer 132 (2013) 2884.

Ms. Wan Qi Lim was born in Singapore in 1992. She has just completed her Bachelor of Science (Honours) in Chemistry at the National University of Singapore. Her research interests include the development of nanoparticles for biodiagnostic and electroanalytical applications.

Dr Zhiqiang Gao is an associate professor at the Department of Chemistry National University of Singapore. He received his BSc and PhD in Chemistry from Wuhan University. The following years he worked as a postdoctoral fellow at ÅboAkademi University and The Weizmann Institute of Science. After spending three years in the United States and eight years at the Institute of Bioengineering and Nanotechnology, he joined NUS in April 2011. Research in his laboratory currently includes analytical chemistry, electrochemistry, biosensors, nanomaterials and energy storage materials.